(4)

DTIC FILE COPY

SIXTH QUARTERLY REPORT

FOR THE PROJECT

"COMPOSITE CERAMIC SUPERCONDUCTING
WIRES FOR ELECTRIC MOTOR APPLICATIONS"

PRIME CONTRACTOR

CERAMICS PROCESS SYSTEMS CORPORATION
155 FORTUNE BOULEVARD
MILFORD, MASSACHUSETTS 01757

31 JANUARY 1990

DTIC
S ELECTE
MAR 0 1 1990
B D

CERAMICS
PROCESS SYSTEMS

90 02 27 089

SIXTH QUARTERLY REPORT

FOR THE PROJECT

"COMPOSITE CERAMIC SUPERCONDUCTING
WIRES FOR ELECTRIC MOTOR APPLICATIONS"

PRIME CONTRACTOR

CERAMICS PROCESS SYSTEMS CORPORATION
155 FORTUNE BOULEVARD
MILFORD, MASSACHUSETTS   01757

31 JANUARY 1990

CPS 90-001

DARPA ORDER NO: 9525
CONTRACT NO: N00014-88-C-0512
CONTRACT EFFECTIVE DATE: 30 JUNE 1988
CONTRACT EXPIRATION DATE: 31 MARCH 1991
PRINCIPAL INVESTIGATOR: JOHN W. HALLORAN
                                         (508) 634-3422

Prepared for
DEFENSE ADVANCED RESEARCH PROJECTS AGENCY
1400 Wilson Boulevard
Arlington, VA   22209

OFFICE OF NAVAL RESEARCH
800 North Quincy Street
Arlington, VA   22217-5000

APPROVED FOR PUBLIC RELEASE: DISTRIBUTION IS UNLIMITED

DTIC
ELECTE
S MAR 0 1 1990
B D

REPORT DOCUMENTATION PAGE

1. AGENCY USE ONLY (Leave blank)	2. REPORT DATE 31 January 1990	3. REPORT TYPE AND DATES COVERED Technical Report 1 Oct – 31 Dec 1989

4. TITLE AND SUBTITLE

Composite Ceramic Superconducting Wires for Electric Motor Applications

5. FUNDING NUMBERS

N00014-88-C-0512

6. AUTHOR(S)

J. W. Halloran

7. PERFORMING ORGANIZATION NAME(S) AND ADDRESS(ES)

Ceramics Process Systems Corporation
155 Fortune Boulevard
Milford, MA   01757

8. PERFORMING ORGANIZATION REPORT NUMBER

CPS 90-001

9. SPONSORING / MONITORING AGENCY NAME(S) AND ADDRESS(ES)

Defense Advanced Research Projects Agency
1400 Wilson Boulevard, Arlington, VA   22209

Office of Naval Research
800 North Quincy Street, Arlington, VA   22217-500

10. SPONSORING / MONITORING AGENCY REPORT NUMBER

11. SUPPLEMENTARY NOTES

N/A

12a. DISTRIBUTION / AVAILABILITY STATEMENT

Unlimited

12b. DISTRIBUTION CODE

13. ABSTRACT (Maximum 200 words)

This report describes progress on developing Y-123 wire for an HTSC motor. The wire development activity includes synthesis of Y-123 powder, spinning polymer-containing "green fiber", heat treating the fiber to produce metallized superconducting filaments, and characterizing the electrical properties of the filaments. Green fiber is produced in lengths up to 1.5 kilometers, and metallized as "green clad" fiber at lengths of 0.5 kilometers. The green clad fiber is converted to silver-clad superconducting wire by a sintering operation. The sintered wire has a $J_c(77°)$ up to 2800 A/cm² in self field, dropping to low values in magnetic fields. Directional solidification efforts are underway to improve the critical current density.

The construction of the first prototype HTSC homopolar motor is in progress. The design specifies a 575 ampere-turn HTSC coil. The current collection system has been tested in liquid nitrogen. Motor performance has been predicted based on actual $J_c(B)$ behavior of wire samples. Motor power and losses have been calculated. The efficiency of this initial machine is limited by the magnetic fields obtainable from present HTSC wire coils.

14. SUBJECT TERMS

Superconductor, ceramic, motor, wires, Composite Materials

15. NUMBER OF PAGES

80

16. PRICE CODE

17. SECURITY CLASSIFICATION OF REPORT	18. SECURITY CLASSIFICATION OF THIS PAGE	19. SECURITY CLASSIFICATION OF ABSTRACT	20. LIMITATION OF ABSTRACT
Unclassified	Unclassified	Unclassified	

COMPOSITE CERAMIC SUPERCONDUCTING WIRES FOR ELECTRIC MOTOR APPLICATIONS

EXECUTIVE SUMMARY

This report describes progress on producing Y-123 wire for an HTSC motor. Wire development focussed process improvement and scale-up. During the down time associated with a major expansion of the continuous sintering furnace, efforts were aimed at optimizing the sintering process of one meter-long wires. The scope of materials was widened beyond phase pure Y-123, as we explored Y-123 alloyed with other phases, the newer Y-124 material, and BiSCCO powders.

Good progress was made in the green fiber areas. A 1.5 kilometer spool of continuous 125-micron fiber was produced, representing nearly a five-fold increase in fiber length. Green fiber braiding, necessary for multifilamentary wire, progressed from eight-filament round braids of 175-micron fiber to sixteen filament flat braids of 125-micron fiber.

The green cladding operation was significantly improved, as silver alloy coatings were produced with much better adhesion, thickness control, and quality. The scale of the green cladding operation was increased more than ten-fold with the production of a 0.53 kilometer long continuous green clad fiber. Using meter-long samples, the burnout and sintering conditions for bare fiber and clad wire were systematically explored. This led to improvements in transport critical current density to values as high as 2800 A/cm^2. Design was completed and construction begun on a 3.3 meter long extension to the continuous sintering furnace to increase the length of the heated sections by more than a factor of five, adding five more controlled temperature zones. With the increased residence time binder burnout and sintering can be done in a single pass, which can increase the production rate of continuously sintered wire by a factor of 8-16.

A more reliable specimen mounting method provided faster feedback data on the effect of processing conditions on J_c, and encouraged measurements of many replicate specimens. The multiple replicate data is used to determine the statistical variation of J_c. Magnetic susceptibility measurements are being done as a routine procedure.

Efforts increased on development of melt processing to produce high critical current density wire. A directional solidification program is beginning involving laser melting at Arthur D. Little with crystal growth and characterization support from Oak Ridge National Laboratory. Rapid thermal processing developments continue in collaboration with Sandia National Laboratory.

The construction of the first generation drum homopolar motor is in progress. A design for a nominal 575 ampere-turn HTSC coil has been specified. The performance of the brush and slip ring current collection system has been tested in liquid nitrogen. Torque and motor performance has been calculated from finite element modeling of flux and current distribution.

Motor performance is predicted using reduced magnetic field levels based on the actual $J_c(B)$ behavior of wire samples. Motor power and losses have been calculated. The efficiency of the first machine is limited by the small magnetic fields obtainable from present HTSC field coils.

ii

TABLE OF CONTENTS

TABLE OF CONTENTS

LIST OF FIGURES

v

LIST OF FIGURES

LIST OF FIGURES

COMPOSITE CERAMIC SUPERCONDUCTING WIRES FOR
ELECTRIC MOTOR APPLICATIONS

JOHN W. HALLORAN
PRINCIPAL INVESTIGATOR
CERAMICS PROCESS SYSTEMS CORPORATION
MILFORD, MASSACHUSETTS 01757

SECTION 1

GENERAL INTRODUCTION

This Sixth Quarterly Report covers activities during October through December 1989, on a program to develop high temperature superconducting wire by cladding $YBa_2Cu_3O_7$-x (Y-123) ceramic fibers with metal, and to use this wire to build a superconducting motor. This program is being carried out by three subcontractors: an affiliate of Ceramics Process Systems, CPS Superconductor Corporation (CPSS) is charged with development of the wire; the fiber spinning technology is being developed with Albany International Research Corporation (AIResCo); and the Emerson Motor Division (EMD) of Emerson Electric is building the superconducting motor. Another contributing organization is the University of Wisconsin Applied Superconductivity Center. During this quarter there were important collaborative developments with Sandia National Laboratory, Los Alamos National Laboratory, and Arthur D. Little Inc.

The status of the program is compared with individual tasks of the revised Statement of Work in Figures 1.1.1, 1.1.2, and 1.1.3, which show timelines for the major fiber and wire development tasks.

The following sections describe in detail the progress on the wire manufacturing task and the motor design task. Section 2 covers all aspects of

the wire manufacturing development, including the fiber spinning work conducted at Albany International Research Corporation in Mansfield, Massachusetts, and the Y-123 powder production, sintering, cladding, and characterization work conducted at CPS Superconductor in Milford, Massachusetts. Section 3 outlines the HTSC motor design activities at Emerson Motor Division in St. Louis, Missouri.

```
        1988          1989                          1990                         1991
        J A S O N D J F M A M J J A S O N D J F M A M J J A S O N D J F M
          1  |  2  |  3  |  4  |  5  |  6  |  7  |  8  |  9  | 10  | 11  |
                                              .
                                              .
                                              .
        Rh-P dry                              .
        spin fiber                            .
        [=======---]                          .
              CPSS dry spin fiber             .
FIBER         [=====================------]
DEVLP                                         .
        BaTiO₃ melt spinning
        [========================-------------
                                              .
                  Y-123 melt spinning
              [=========================================]
                                              .
                      Green  fiber. braiding
                  [=======================]
                                              .
                                              .
          1  |  2  |  3  |  4  |  5  |  6  |  7  |  8  |  9  | 10  | 11  |
```

Figure 1.1.1   Revised Project Schedule for Fiber

```
1988          1989                        1990                          1991
J A S O N D J F M A M J J A S O N D J F M A M J J A S O N D J F M
  1   |   2   |   3   |   4   |   5   |   6   |   7   |   8   |   9   | 10   | 11   |
                                        .
Lab sinter                              .
[===========================--]         .
                                        .
              RTC furnace               .
              [=====================]   .
                                        .
WIRE                                    .
                                        Ribbon wire
DEVLP                                   .========================
                            ↑ POSTPONE
         Cladding module    RIBBON WIRE
         Design and build               .
         [=======================]
                                        .
Silver coat and co-fire                 .
[=============================------------------]
                                        .
              Silver monofil wire       .
                  [=====================================]
                                        .
  1   |   2   |   3   |   4   |   5   |   6   |   7   |   8   |   9   | 10   | 11   |
```

Figure 1.1.2   Revised Project Schedule for Wire Tasks.
                Note that Ribbon Wire had been postponed in favor
                of monofil wire

```
           1988         1989                        1990                        1991
           J A S O N D J F M A M J J A S O N D J F M A M J J A S O N D J F M
            1  |  2  |  3  |  4  |  5  |  6  |  7  |  8  |  9  | 10  | 11  |
MOTOR             application                     .
DELVP               study                         .
                [===========]                     .
                                                  .
           define properties              build test equip
           [=========================]     [================]
                                                  .
                                           test short
                                             wire        test coils
                                           [======][===================]
                                                  .
                                           design    fabr    test
                                           motor     motor   motor
                                    [=================][=======][===============]
                                                  .
                                           advanced motor design
                                                  ↑
                                               postpone
                                                  .
            1  |  2  |  3  |  4  |  5  |  6  |  7  |  8  |  9  | 10  | 11  |
```

Figure 1.1.3   Project Schedule for HTSC Motor Task

SECTION 2

WIRE FABRICATION

DAVID CHANDLER, JOHN HALLORAN, JAMES HODGE, LORI JO KLEMPTNER,
MATTHEW NEAL, MARK PARISH, HYUN PARK, MICHAEL PARKER, AND VIREN PATHARE
CPS SUPERCONDUCTOR CORPORATION

GEORGE BAKIS, DANA EAGLES, WESLEY ISHIDA, AND STEPHEN TIERNAN
ALBANY INTERNATIONAL RESEARCH CORPORATION

2.1   Introduction and General Comments

During this quarter the predominant activities involved improving each of the major process steps, increasing the length of green and green clad 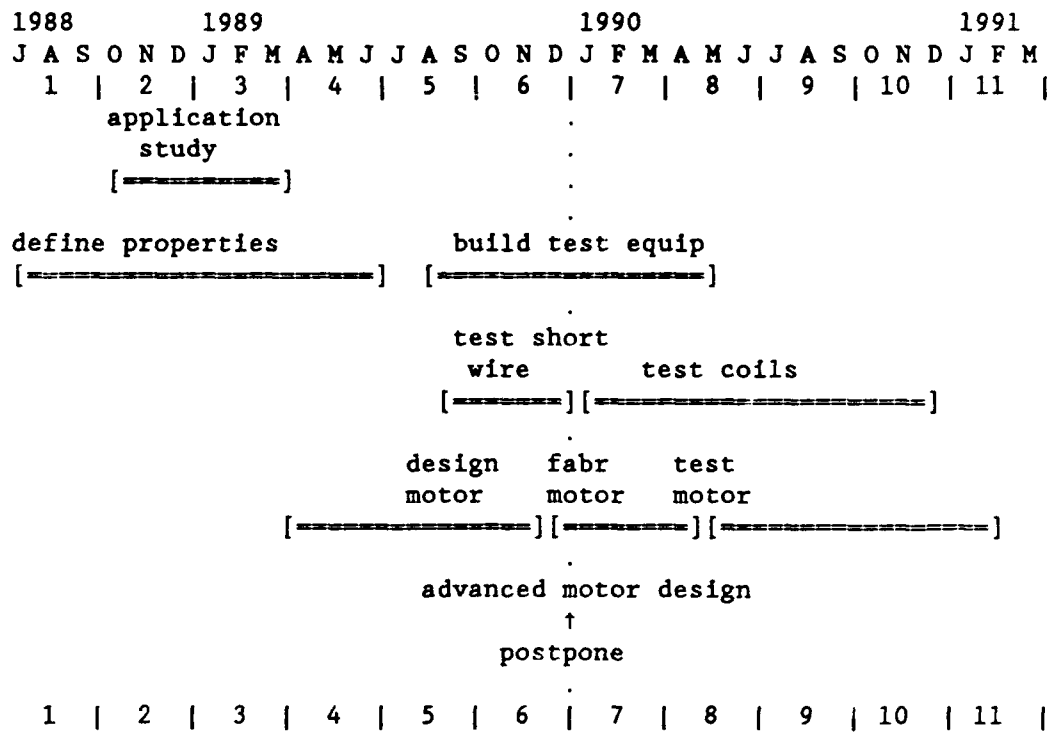fiber into the kilometer range, building an extension on the sintering furnace, and correlating critical current density with processing parameters to begin optimization of the sintering schedule. The nature of the work was rather different than the previous quarter, when the major task was producing continuously sintered silver clad monofilament wire, and much of our energies were devoted to overcoming practical problems associated with reel-to-reel wire sintering. The continuous sintering work pointed out some deficiencies with the RTC belt furnace. Inconveniently slow belt speeds were needed to conduct burnout in the relatively short hot zone, and two or three separate reel-to-reel passes were required for binder burnout and sintering. To overcome this problem we designed and began to build an extension to the belt furnace. Further continuous sintering work was postponed until the furnace extension was ready. We took advantage of the furnace down time to improve the coating process and conduct extensive matrix experiments on sintering.

There has been progress in the electrical properties of the wire. With the best processing conditions, critical current density values as high a 2800 A/cm² have been obtained. More data have been obtained on the statistical variation of J_c, and we have begun to correlate the transport properties with magnetic susceptibility.

The detailed progress reports for each of the four wire process steps are presented in Sections 2.2 through 2.5.

2.2   Fiber Preparation

2.2.1   Introduction

The green fiber development this quarter focussed on improving the spinning process by controlling each process step more carefully to strictly eliminate variability in the process. Polyvinyl butyral was evaluated as a promising carrier polymer which could be superior to high density polyethylene in both spinnability and burnout behavior. Significant progress was made in the area of green fiber braiding, including the introduction of a flat braider for producing 16-filament flat braids, braiding of 125-micron green fiber, and braiding of green clad 125-micron fiber   Finally, the scale of the fiber production was increased to produce longer spools of fiber, including a continuous fiber 1.5 kilometers long.

2.2.2   Powder production

Production of Y-123 powder continued routinely to supply project needs. About 20 lots of powder, amounting to some 12 kilograms were produced. The present production rate is quite adequate for present, so no significant scale-

up activities were undertaken. A series of experiments were done to prepare powders with different particle size distributions.

Production was begun on a variety of other compounds to support the operation. In the YBCO system, mixtures of Y-123+CuO admixtures were prepared. To support a broader exploration of this system, quantities of Y-211 and barium cuprate were produced to allow us to prepare fibers consisting of phase assemblages around the Y-123 composition. Experimental substitutions of lanthanum, strontium, and fluoride were explored.

Synthesis of powders in the BiSCCO system was begun in earnest during this quarter. Efforts were motivated by the claims by Chandrachood et al.[1] and Liu Hongbao et al.[2] of 132K zero resistance in Sb-doped BiSCCO. Unfortunately we have not been able to reproduce their results. After learning that other groups had failed to see any hint of a 132K superconductor in the Bi(Sb)SCCO system, we abandoned the effort. Several runs were made to produce conventional 110K Bi(Pb)SCCO material for fiber spinning. These fibers will be spun in the next quarter.

2.2.3 Green fiber spinning

During this quarter 22 spinning experiments were carried out to supply the program with standard fiber, evaluate new polymer systems, and produce fibers from experimental powders. More emphasis was placed on process control. One of the highlights of the fiber spinning activity was the production of the longest fiber to date-- a continuous 125-micron fiber more than 1.5 kilometers long. Figure 2.2.1 is as photograph of the spool. This fiber was spun using the standard HDPE formulation at 50 volume percent solids loading.

Higher solids loading should improve binder burnout and sintering behavior. Using the standard HDPE formulation, it was possible to produce 125-micron fiber at a solids loading of 60 volume percent. At this solids loading the compound is significantly more difficult to extrude. At this stage of development, the 60% fibers were difficult to reproduce, so more development work is underway. Initial feedback on these fibers show improved sintering and electrical performance.

2.2.3.1 Alternate Polymer Systems

Polyvinyl butyral and acrylic resins were further evaluated as alternatives to the HDPE. Both of these systems possibly would allow faster binder burnout during sintering, and also might have benefits during fiber processing.

Polyvinyl butyral (PVB) is an acidic polymer, which theoretically would offer better adhesion on the basic surface of powders like Y-123 and barium titanate, promoting dispersion, improved rheology and higher green strength. Unlike HDPE, PVB is an amorphous polymer, which might allow successful cold drawing to permit finer fiber diameters. Recall that previous experience with finer diameter drawn HDPE fibers were frustrated by excessive axial shrinkage during initial heating. It was felt that much of the shrinkage due to increased molecular orientation and crystallization of the HDPE during drawing, which relaxed during heating. An amorphous polymer like PVB would not experience crystallization during drawing.

PVB-based fibers were spun with barium titanate and Y-123, using our usual technique of evaluating new grades of resins with the less expensive barium titanate. The spinnability and green properties of the fibers were excellent.

Easily handable barium titanate fibers were produced with diameters as fine as 75-microns. Green Y-123 fibers were produced with several PVB-based polymer blends. These are presently being evaluated. They appear to have marginally better burnout properties, and satisfactory sintering behavior. An extensive matrix comparing the critical current as a function of sintering condition is now being conducted. The preliminary indication is that the PVB fibers achieve about half the J_c of the best HDPE fibers. More work is underway.

A series of high molecular weight methyl methacrylate resins and copolymers and butyl/isobutyl methacrylate were evaluated. This work differed from previously-reported acrylic evaluations in the choice of plasticizer. Improved additives have allowed us to make continuous 125-micron fiber from some of the acrylic grades, but so far the spinnability and green fiber properties are inferior.

2.2.3.2 Y-123 Fibers with Internal Silver Dispersoids

Several attempt have been made to prepare Y-123 fibers containing metallic silver admixtures. Simple mechanical mixtures of Y-123 powder with silver powder were unsatisfactory. Dry blended powders produced material with rather non-uniform silver distribution, probably reflecting agglomeration of the Ag particles. Attempts to ball mill silver powder with Y-123 were unsuccessful, as the soft silver powder deformed and agglomerated, rather than mixing homogeneously with the ceramic. To overcome these problems we prepared mixtures of Y-123 with silver oxide, Ag_2O. This caused an unexpected problem. During compounding of the Y-123+Ag_2O with the molten polymer blend, the blend suddenly ignited and created a rather spectacular (and alarming) pyrotechnic display. After extinguishing the blaze, this spin run was abandoned.

Subsequent analysis indicates that the silver oxide behaved as an internal solid oxidant for combustion of the organic binders. After ignition by the reaction:

$$Ag_2O + C_xH_y - Ag + CO_2 + H_2O$$

there was apparently a secondary combustion in which the CuO component of the ceramic served as the oxidant. To avoid similar problems in the future, we have developed a DSC thermal analysis procedure to screen potentially hazardous new compositions. We have returned to mechanically mixed silver powder with Y-123 powder, with more careful blending, to prepare these internal composite fibers. They will be spun in the following quarter.

2.2.3.3 Copper Oxide Doped Green Fibers

Green fiber containing 1%, 3%, and 10% (by weight) copper oxide additions were prepared for sintering and rapid thermal processing experiments. The fibers with 10% CuO were also used to prepare Y-124 fiber. The fibers were formulated with the standard HDPE-based polymer system. These spins were curious in that they exhibited die swell to a much greater extent than had been previously experienced with this system. Fiber spun through a 125-micron die swelled to diameters of 150-175-microns after exiting the die. Die swell is typically associated with viscoelastic relaxation of the carrier polymer. It is not clear why the addition of a second powder component- ball milled CuO- would affect polymer relaxation.

These CuO-doped fibers proved to be inferior to the previous fibers made with additions of 5% CuO. The conventional sintering behavior was not improved. In rapid thermal processing (RTP), the 1% and 3% fibers were quite similar to undoped fibers, while the 10% CuO fibers produced too much liquid phase. Apparently 5% CuO is close to the optimum for RTP.

2.2.3.4 Preparation of Y-124 Filaments

Recently Jin et al.[3] reported a simple synthesis for $YBa_2Cu_4O_8$ (Y-124) by heating a mixture of Y-123 powder and CuO powder in flowing oxygen for 12 days at 810°C. This suggested an opportunity to prepare Y-124 filaments from our existing Y-123+10 weight percent CuO material. This composition represents a CuO/Y-123 molar ratio of 0.84, which is close to the 1:1 molar ration for Y-124. Samples of mixed powder, presintered (915°C, 30 minutes) filaments, and filaments after a 400°C binder burnout were all annealed at 810°C for 12 days in flowing oxygen. After this anneal, XRD of the powder showed nearly complete conversion to Y-124. The filaments had much less conversion, with XRD patterns consistent with about equal fractions of Y-123 and Y-124. These specimens will be used for RTP experiments.

2.2.4 Braiding of Y-123 green fibers

A braiding machine capable of producing flat braids was obtained and set up during the quarter. Flat braids are more appropriate for the multifilamentary wire than the tubular round braids we had previously produced. Excellent progress has been made in handling the green fiber more gently during the braiding process, allowing the standard 125-micron green fiber to be braided with relatively few breaks. About 10 meters of a 16-filament braid were

successfully produced with bare 125-micron fiber. Figure 2.2.2 shows the 16-filament braid in the green state. A preliminary experiment indicated that the braid would could be sintered, but no further work was done on sintering of bare braids, as the filament-filament contact defeats the purpose of multifilamentary wire. The next experiment was on silver coated green clad fiber. About 540 meters of 125-micron fibers were coated as described in the following section. The green clad fiber was re-spooled onto 16 smaller spools to supply the braiding machine. Braiding was successful. The handling and manipulation of the green clad fiber did not damage the cladding, and the presence of a few "bead" cladding defects did not cause breakage.
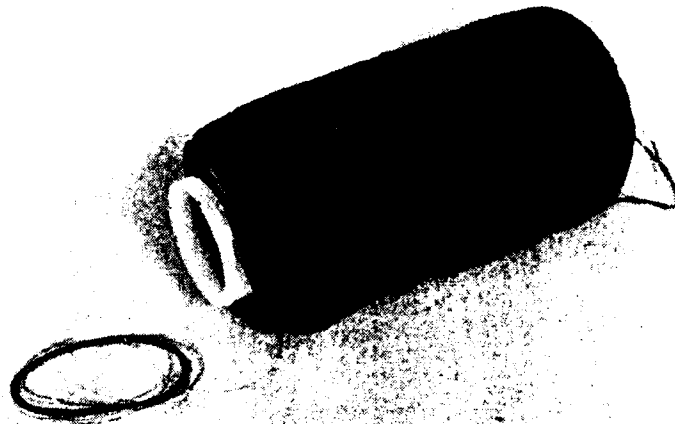
Figure 2.2.1   Photograph of 1.5 Kilometer Spool of Y-123 Green
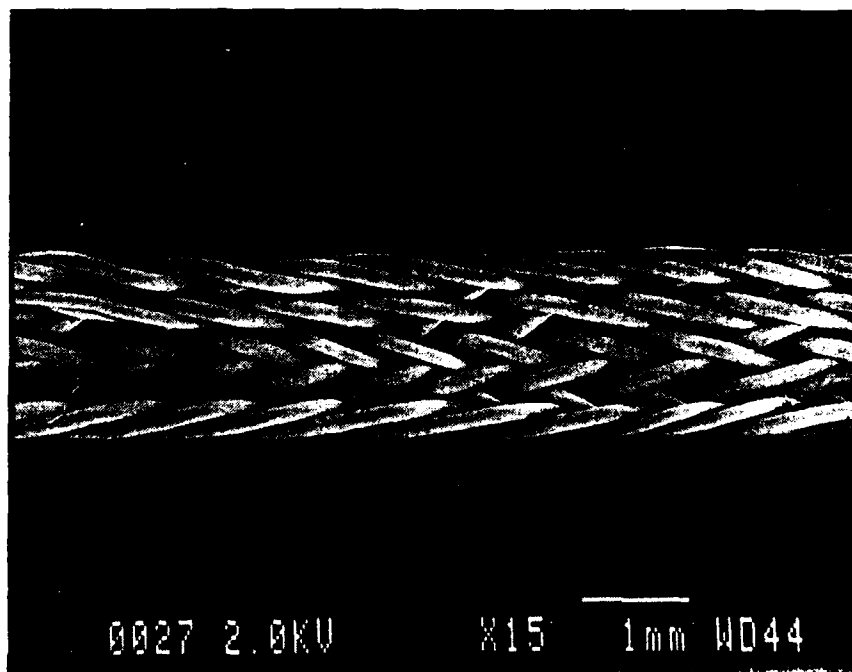
Fiber

0027 2.0KV   X15   1mm WD44

Figure 2.2.2   Sixteen Filament Flat Braid of

125-Micron Y-123 Green Fiber

2.3   Sintering and Cladding

The quality of the sintered wire and filament, in terms of microstructure and electrical properties, is the ultimate parameter governing our choice of each of the processing conditions.   Each process variation is judged by its influence on the quality of the sintered material. Variations in the powder characteristics, composition, fiber formulation and spinning conditions, green cladding alloy composition, formulation, thickness, and coating conditions, etc., are related to sintered density, microstructure defects, and transport critical current.   In addition, the binder burnout and sintering conditions are being investigated to improve wire quality and increase burnout and sintering rates. Consequently, we tend to carry out a large number of sintering experiments. During this quarter, about 280 individual sintering experiments were conducted, often with multiple specimens.

2.3.1   Cladding and co-firing

The cladding and sintering operations have been effectively combined with the emphasis on monofil wire. Most of the sintering experiments involve co-firing of "green clad" wire, i.e., the green fiber coated with the powder metallurgical silver alloy powders. Bare fiber is sintered only in exploratory experiments aimed at evaluating new fibers or establishing baseline data for Y-123 fiber properties without the additional variable of the silver alloy cladding.

2.3.1.1 Green Cladding

The green cladding coating process was significantly improved and scaled-up during this quarter. An extensive optimization effort was undertaken to improve the quality and control of the coating formulation. This included evaluating alternative metal powders, binders, and processing aids. The aim is a well control, smooth coating, with excellent uniformity, adherence, and concentricity. The coating apparatus and process was also improved with the principal aim of producing longer spools of defect-free green clad fiber. Figure 2.3.1 shows two green clad fibers, illustrating the range of green clad thicknesses commonly used at present. The uniformity, concentricity, and smoothness of the coatings are typical of the current state of development. (Note that the slight ovality is caused by cutting the clad fiber with a razor blade. The fiber is actually quite round.)

In the last quarterly report, we discussed a problem with the adhesion of the green cladding on the polyethylene-based green fiber. This was overcome by reformulating the polymer system of the coating to improve adhesion. This eliminated the coating-fiber adhesion problem, but formed a slightly tacky silver coating. The tackiness caused fibers to stick to each other on the spool, which damaged them upon subsequent despooling. The tackiness problem was overcome by using a multilayer cladding, with the first layer formulated for strong adhesion and the final layer a good film former giving a smooth, non-tacky surface. Multilayer green claddings are now being designed to incorporate additional elements of control to tailor the properties of the metallization. The PVB-based green fiber could be green clad with the same formulations used for the HDPE-based fiber.

The principal cladding defects during this period are beads which form during instabilities in the coating process. The beads, typically 1mm thick, form whenever there is a disturbance in the coating operation created by vibrations or transients in the fiber velocity. The frequency of beading was significantly reduced by rebuilding the coating apparatus to eliminate vibrations and redesigning the spooling mechanism to take up the coated fiber immediately past the drying column. A new system has been designed to synchronize the green fiber payout and coated fiber takeup to further improve coating uniformity.

With these improvements we were able to produce much longer green clad fiber. In one instance, 0.53 kilometers of continuous green clad fiber were produced to provide feedstock for 16-filament braids. This is more than a ten-fold increase in green clad fiber length, and indicates that the process is clearly adaptable for manufacture. Before the process is ready for multi-kilometer production, however, the apparatus must be improved to allow unattended operation. At present, the operator must frequently intervene to adjust the coating apparatus, which makes production of long fibers rather tedious.
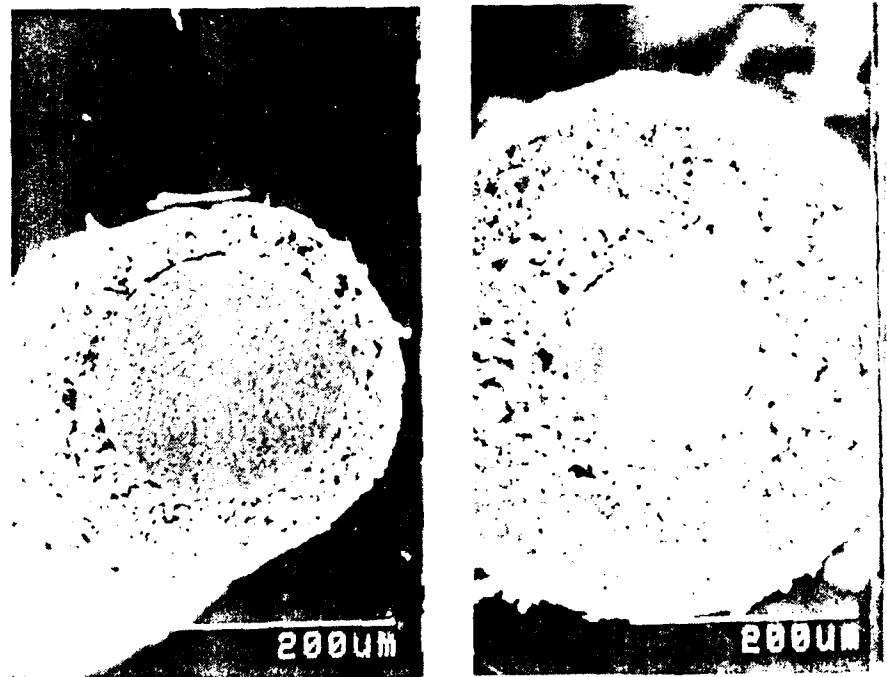
Figure 2.3.1   Cross-Section of Silver Green Clad

Fiber Showing Typical Range of Thickness

2.3.1.2 Co-Firing of Green Clad Fiber

Most of our recent activity has focussed on co-firing of meter-long fibers to establish the effect of temperature and time (express~ l as zone temperature and belt speed) on the microstructure and properties of the wire. Some work was done on continuous sintering, although most of these experiments have been postponed until the new furnace extension is available. Using meter-long specimens duplicates many of the features of continuous sintering, since the fibers are longer than the heating zones, but are much more convenient for systematic experiments.

Binder burnout and sintering can be done as separate steps in the experiments with meter-long green wires. Burnout conditions are explored by varying belt speed and zone temperature in the 200-600°C range, followed by a standard high temperature densification, after which microstructure and properties are characterized. Similarly, the high temperature sintering conditions are explored using constant burnout conditions.

Figure 3.3.2 is a polished cross section of a silver clad wire co-fired at 920°C using our standard 125-micron green fiber and a typical clad thickness. In this case, the sintered wire is about 155 microns in diameter, consisting of a 20-micron silver cladding on a 115 micron Y-123 core. Such a 20-micron cladding thickness provides adequate strength for handling. This corresponds to a Ag/Y-123 volume ratio around 0.77, or a weight ratio of 1.3. The porosity in the Y-123 phase is in the range which corresponds with good electrical properties. The as-fired surface of the clad wire is shown in Figure 2.3.4.

We have for the present adopted two "standard" binder burnout profiles. Both are chosen to be conservative, so that a wide range of parameters can be

accommodated. The burnout profiles have the peak zone temperature set at 400°C and use belt speeds of 1.0 inch per minute for bare fibers (25 minute residence time) and 0.5 inch per minute for green clad fibers (50 minute residence time). The latter speed is chosen to assure that even the very thick silver coatings (above 100 microns) safely survive burnout without defects. This residence time corresponds to a speed of 2 inches per minute in the extended furnace, but would be significantly increased for thinner claddings.

About half of the sintering experiments were conducted to evaluate experimental green cladding conditions and formulations. Typically the multilayer green claddings were examined over a range of thickness. The results of these sintering tests were the feedback for the cladding development. Many of the other sintering runs were aimed at optimizing sintering conditions for the fiber itself.

A large matrix experiment was begun during this quarter to assess the effect of temperature and belt speed (i.e., residence time) for bare fibers prepared at 50 volume percent Y-123 in the HDPE system, 60 volume percent Y-123 in the HDPE system, and 50 percent in the PVB system. After a standard oxygen anneal[1] the transport critical current density (self field) was measured at 77K. Since J_c values are very scattered, replicate specimens were measured, with sample sizes between 3 and 22. Figure 2.3.5-2.3.7 are histograms showing the frequency of J_c values for these three types of filaments sintered at 920, 950, and 970°C at a belt speed of 2.5 cm/ minute (or 30 minute residence time). The general trend is for higher J_c values to be obtained at lower sintering

---

[1]. The present standard oxygen anneal is to heat quickly in flowing oxygen to 820°C, then cool to 550°C at 150°C/hr, hold at 550°C for 10 hours, then furnace cool.

temperature. The 60 volume percent HDPE filaments consistently displayed higher critical current densities, reaching values around 2400 A/cm^2 when sintered at 920°C. Sintering at 950°C reduced J_c to around 1000 A/cm^2, and the values were highly scattered. At 970°C the value fell to 250 A/cm^2. The 50% HDPE specimens were consistently lower than the 60% specimens, while the PVB filaments were distinctly inferior. More data is now being collected at different belt speeds.

The experiments involving a large number of replicated provide an opportunity to examine the statistical variations in the J_c data. A few of these seem to have an approximately normal distribution of values. For example, the 60%/950°C data set of 22 widely scattered values are excellently fit with a normal distribution having a mean of 680 A/cm^2 and a standard deviation of 311 A/cm^2. The 50%/950°C data set are fairly well represented with a mean of 970 A/cm^2 and a standard deviation of 442 A/cm^2. The 60%/920°C data, which had the higher critical currents, fit a normal distribution less satisfactorily, giving a mean of 2290 A/cm^2 and sample standard deviation 288 A/cm^2. The origin of the scatter in J_c values is presently obscure. We continue to collect data to help us characterize the statistical variations, since a well-established distribution function is needed to predict long wire critical currents from short wire tests.
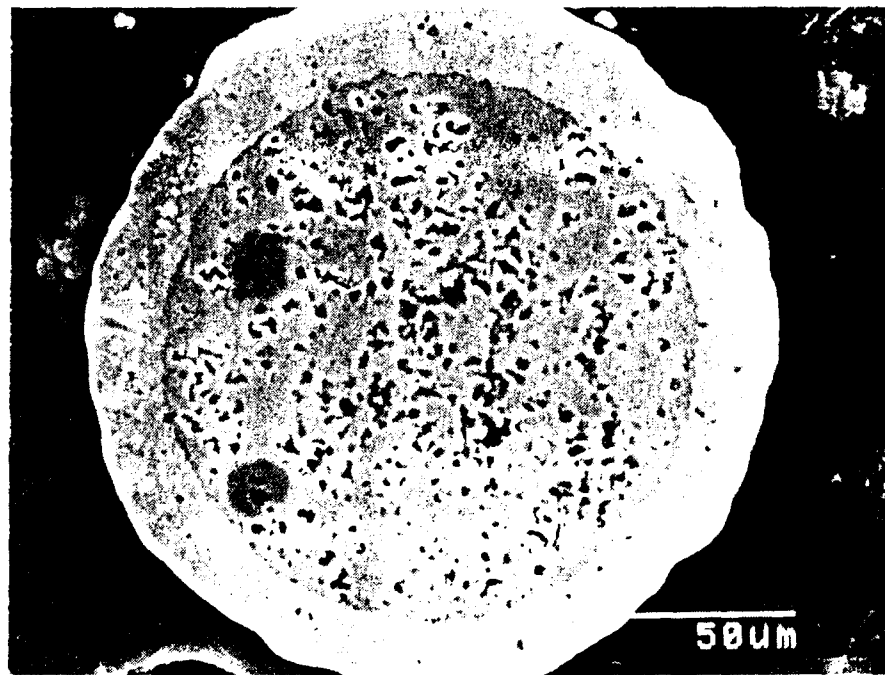
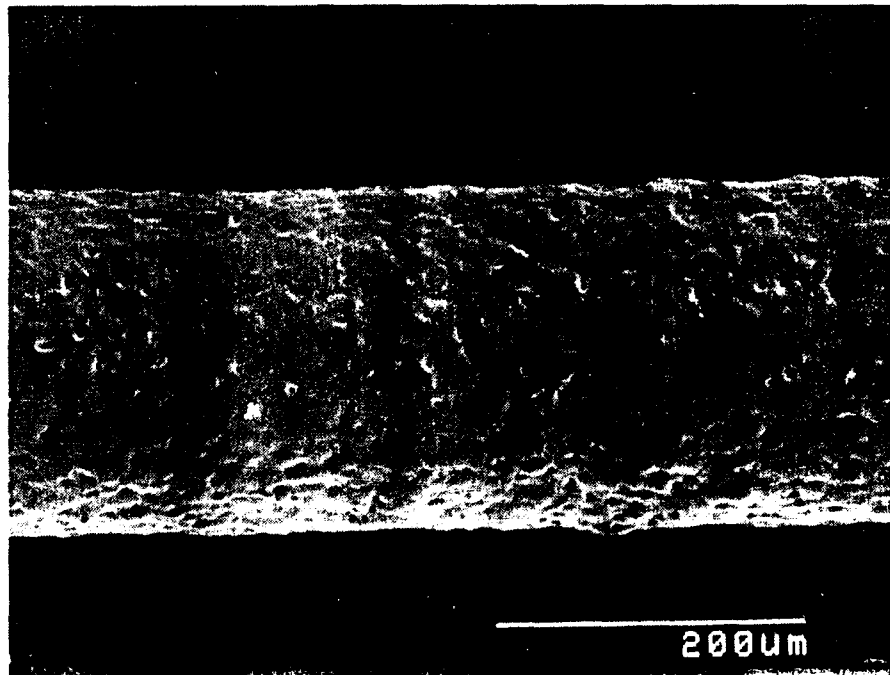Figure 2.3.2   Polished Cross-Section of Co-Fired Wire

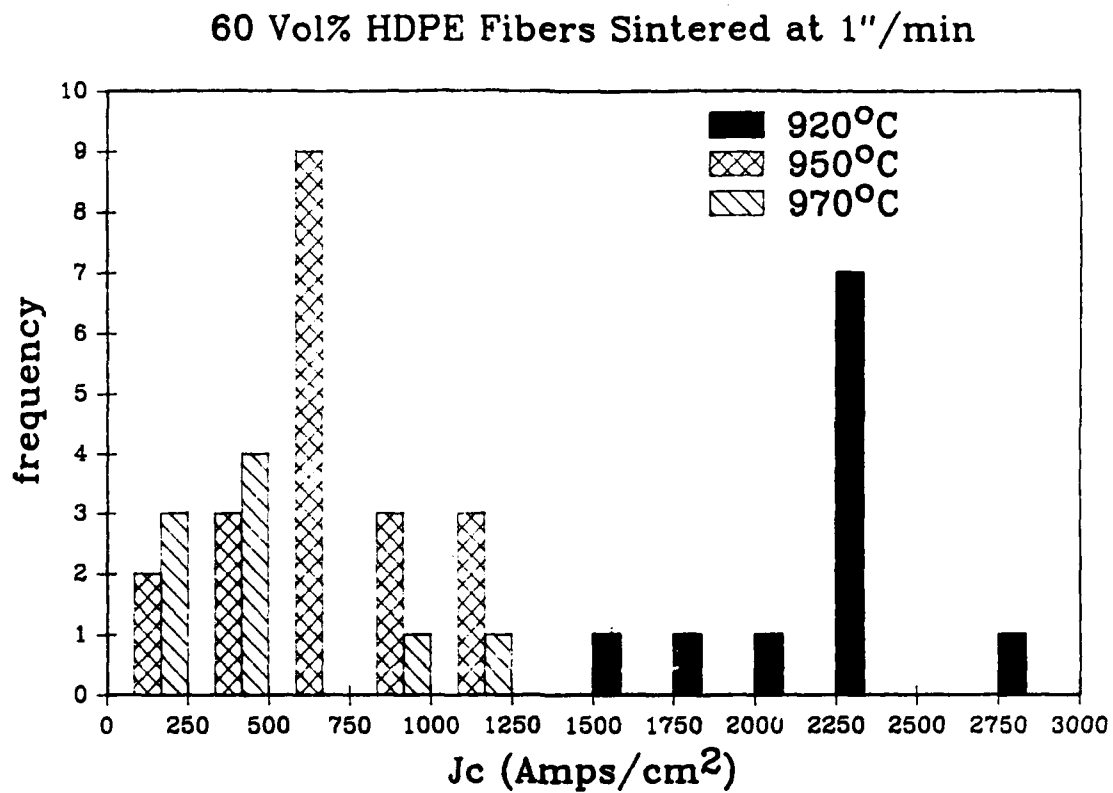Figure 2.3.3   Silver Surface of Clad Wire

60 Vol% HDPE Fibers Sintered at 1"/min

Figure 2.3.4   Distribution of 77K Transport Critical Current

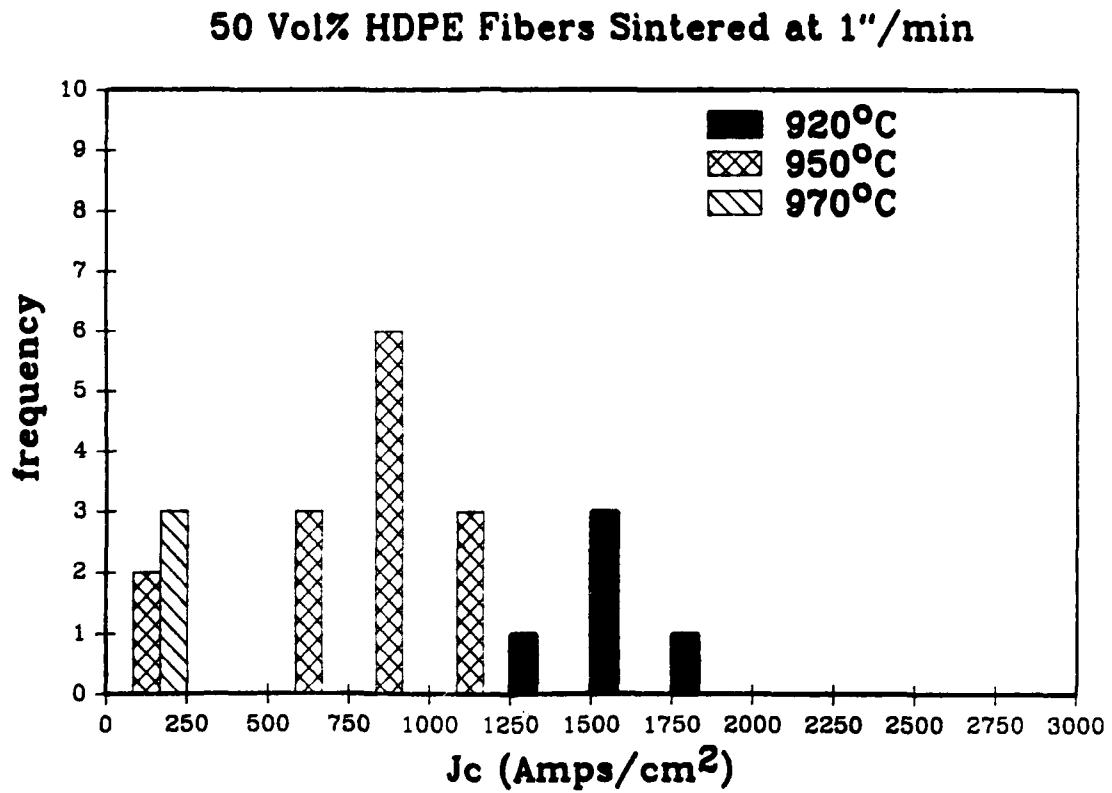Density for 60vol% HDPE Filaments Sintered

30 minutes at 920, 950, and 970°C

50 Vol% HDPE Fibers Sintered at 1"/min

Figure 2.3.5   Distribution of 77K Transport Critical Current

Density for 50vol% HDPE Filaments Sintered

30 Minutes at 920, 950, and 970°C

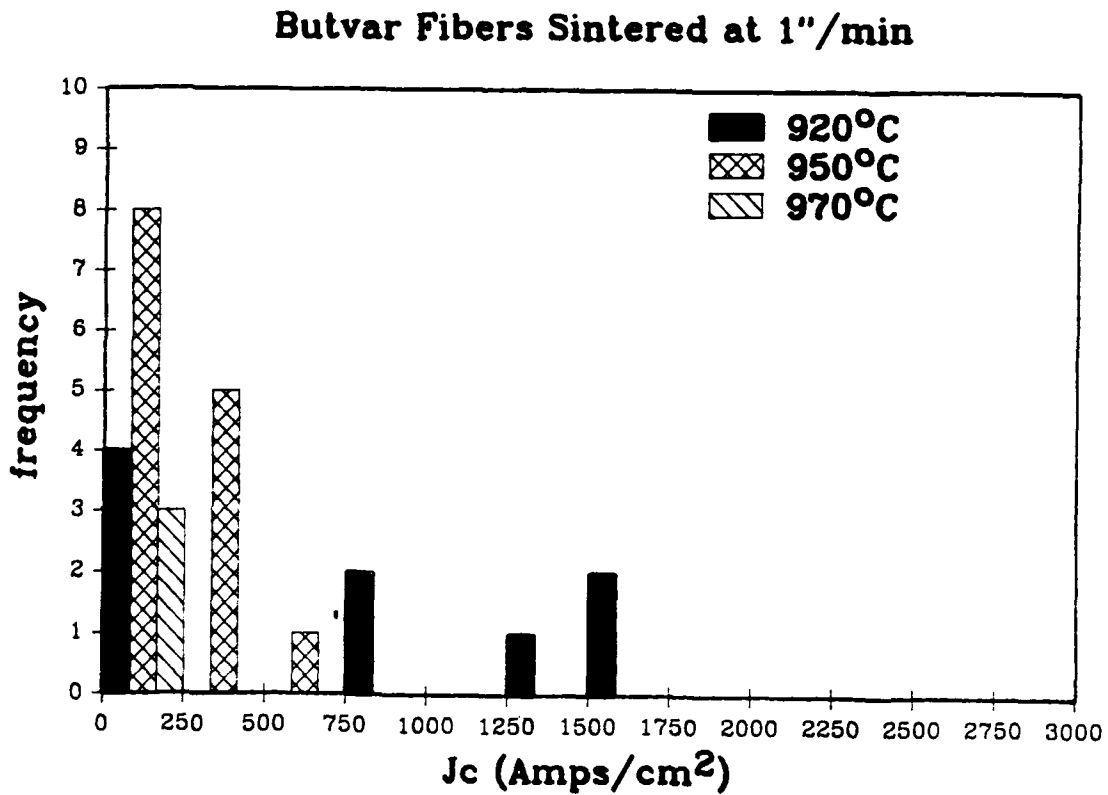**Butvar Fibers Sintered at 1"/min**

Figure 2.3.6   Distribution of 77K Transport Critical Current
Density for 50vol% PVB Filaments Sintered
30 Minutes at 920, 950, and 970°C

2.3.1.3 Nitrogen Sintering

Sintering in a nitrogen atmosphere was de-emphasized this quarter. Previously we had tried to extend the peak temperature for the pure silver cladding by sintering in flowing nitrogen with an oxygen content below 300 ppm, to move up the effective silver melting point[2] and lower the sintering range of the Y-123. This was done with some limited success. Early in this quarter we found better behavior in wires sintered in air at 920°C, so we concentrated on air-sintering and set aside for the present nitrogen-sintering experiments.

2.3.1.4 Anomalous Melting of the Silver

For a period during this quarter we began to find unusual defects in silver cladding on sintered wires, which appeared to be localized bare spots. These were eventually traced to bare spots forming from otherwise apparently perfect green cladding after the usual binder burnout at 400°C in air. Closer examination showed that, in occasional local regions, the silver had obviously melted, even though the furnace temperature never exceeded 400°C. The local melting problem was less severe upon faster heating, or with thicker cladding. It seemed to be associated with local ignition of the polymer binder in the green cladding.

The localized melting was more severe when the binder burnout was conducted in oxygen rather than air. However it could not be entirely suppressed by binder burnout in flowing nitrogen. It occurred also when pre-sintered bare Y-123 filaments were electroded with silver paint dope and fired to sinter on

---

[2]. In air the maximum temperature the silver will tolerate before melting of the $Ag-Ag_2O$ eutectic is about 925°C.

silver electrodes. The reaction was clearly associated with Y-123. As a control, alumina green fibers were green clad, and no melting occurred during binder burnout.

The polymer combustion reaction uses the cuprate as an oxidizer, since alumina green fibers were inert in air, while the cladding on Y-123 fibers melted during heating in essentially oxygen-free nitrogen. It appears that this particular grade of silver powder was catalyzing the combustion of the polymer binder in the green cladding, as the problem does not occur with a lower surface area flake silver powder. With the conventional higher surface area silver powder, the combustion problem was suppressed by changing the binder system of the green cladding to use another grade of the same polymer with more hydroxyl functionality.

2.3.1.5 Embrittlement of Silver-Palladium Cladding

In the previous report we noted that Ag-Pd claddings were mechanically unsatisfactory due to brittleness. The cause of the embrittlement was determined to be a minor amount of rhodium in the alloy. This particular alloy contained 0.5 weight percent Rh, added to inhibit the sintering of the alloy powder. The controlled-sintering rate alloy was being evaluated to improve the match between the silver and Y-123 densification rate. Later we found this was not necessary. Rhodium-free Ag-Pd alloys are not brittle.

2.3.1.6 Reactions with Palladium

We use palladium to increase the melting point of the silver, allowing us to sinter wire above the circa 925°C silver-oxygen eutectic melting point. Previously we reported a deleterious reaction occurring between the Y-123 and

Ag-18Pd alloys co-fired above 970°C, with no apparent problems at lower temperatures. This work has expanded in scope, and revealed extensive reactions at temperatures as low as 875°C.

Two types of experiments were performed using Ag-30Pd alloys. Dry pressed pellets were prepared by mixing Y-123 powder with 50% by volume of one-micron prealloyed powders of silver-30 weight percent palladium. These pellets were passed through the RTC furnace using a belt speed corresponding to 30 minutes at peak temperature. Temperature varied between 875 and 995°C. Identical runs were conducted with 125-micron fiber green clad with the Ag-30Pd alloy. After sintering the pellets were examined by X-ray diffraction. In all cases there was a substantial amount of decomposition of the Y-123 to form barium cuprate, 211, and copper oxide. Visual examination of the specimens indicated partial melting. Control specimens fabricated with pure silver powder had no detectable reaction. Figure 2.3.8 shows semiquantitative (binary standards method) XRD data indicating that about 50wt% of the Y-123 is decomposed in the presence cf Ag-30Pd. The clad wire sintered at 950°C also shows a similar degree of decomposition, as shown by the XRD pattern of Figure 2.3.9.

Presumably the palladium promotes the peritectic decomposition reaction:

$$2 \ YBa_2Cu_3O_7 \rightarrow Y_2BaCuO_5 + 3 \ BaCuO_2 + 2 \ CuO$$
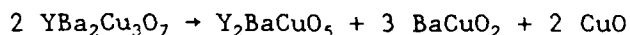
with the barium cuprate and the copper oxide probably liquid at reaction temperature. It is likely that palladium lowers the peritectic decomposition temperature by altering the thermochemical activity of the copper. It is known that copper and palladium alloys have negative deviations from ideality[4], so that palladium would depress copper activity in an Ag-Pd-Cu ternary alloy, and tend to stabilize metallic copper. Perhaps the Ag-Pd alloy extracts a small amount of copper from the Y-123, forming a metallic phase which promotes the stability

of Cu^0. Equilibration of the metallic phase with the oxide phases would favor the more reduced cupric valence states and promote the peritectic reaction. Qualitative EDS analysis of the metallic phase in reacted specimens shows a small amount of copper.

Reactivity seems much less severe with the Ag-18Pd and Ag-15Pd alloys which we more commonly use for cladding. Wires clad with Ag-15Pd show virtually no reaction by XRD after sintering at 950°C. Electrical data also suggest no serious problem. Nonetheless, we will carefully investigate these reactions during the next quarter.
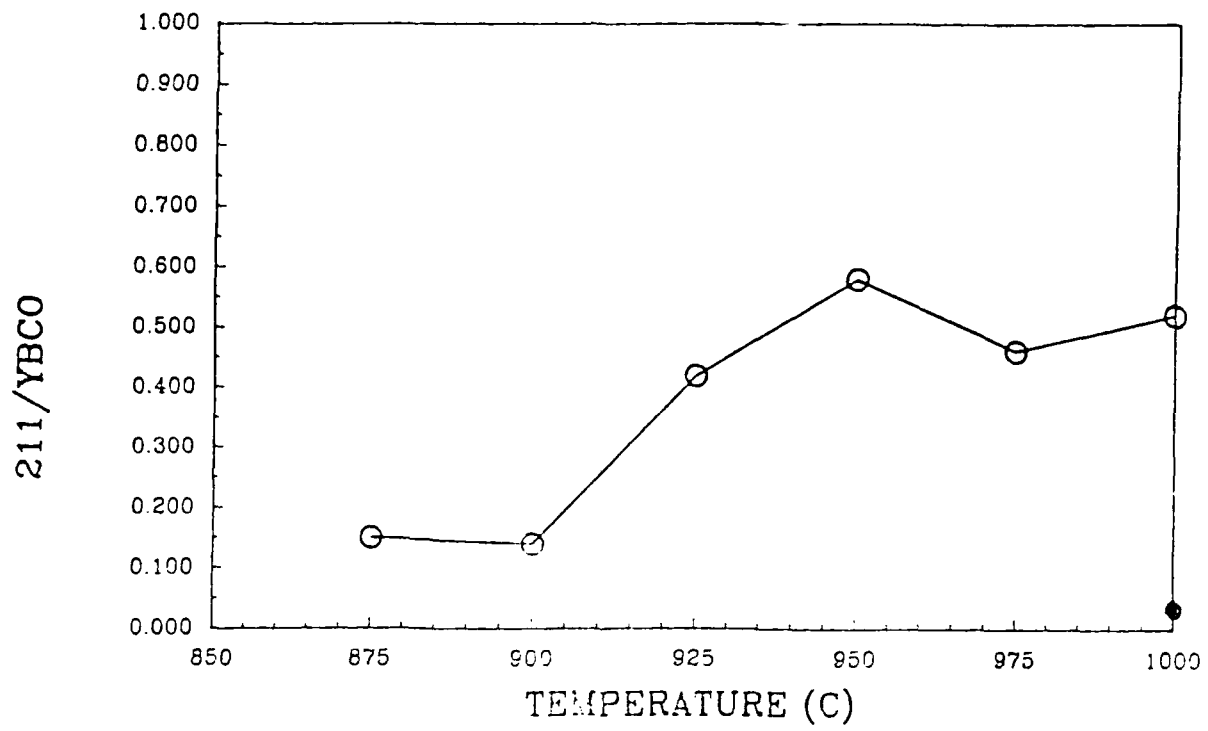
Figure 2.3.7   Semiquantitative XRD Data on Phases formed

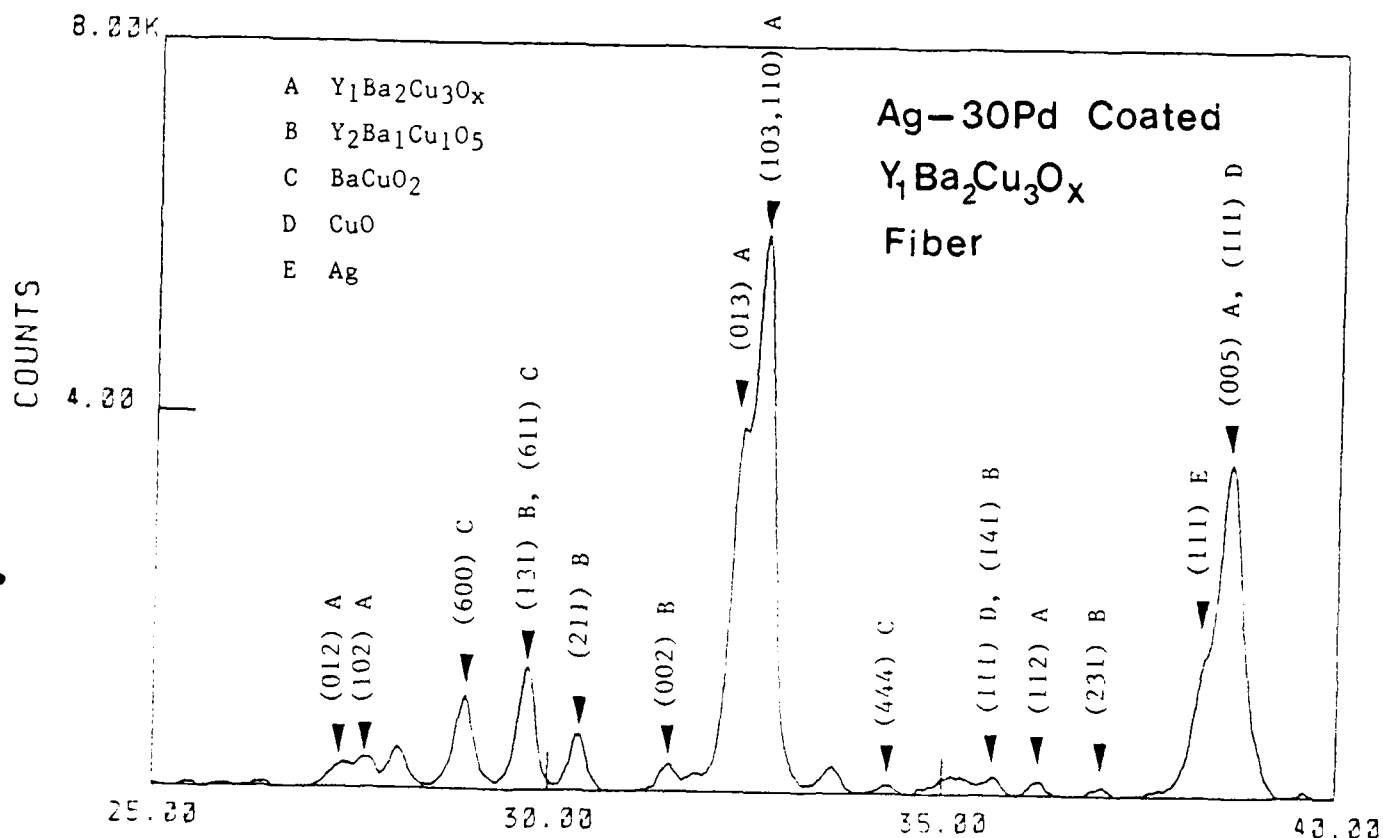by Reaction of Y-123 with Ag-30Pd

Figure 2.3.8   Copper K_α X-Ray Diffraction Pattern of

a Ag-30Pd Wire Sintered 30 Minutes at 950°C

2.3.2   Continuous Sintering

Relatively little direct work was done with continuous wire sintering during this quarter. At the close of the previous quarter we were able to conduct continuous sintering, but at inconveniently slow speeds. The critical step controlling overall production rate was binder burnout. The modified RTC furnace had only 71 centimeters of working hot zone, so as a practical manner binder burnout had to be conducted in several steps with intermediate spoolings between steps. We began designs for a extension to the RTC to conduct the binder burnout.

The as-sintered wire is poorly superconducting. Figure 2.3.10 shows the resistive transition from a continuous sintered wire co-fired with a Ag cladding at 920°C. This wire was sintered in three steps: 1) binder pre-removal pass at peak temperature of 270°C; 2) pre-sinter pass, with temperature zones set from 400-920°C; and 3) second sintering step with all three zones set at 920°C. After the pre-sintering pass (number 2), the wire is not superconducting. The as-sintered wire after the second sintering pass (number 3) has a broad transition with onset at 88K and zero resistance at 80K. This wire cooled from sintering temperature at a rate of 100°/minute, so it is surprising that the material is superconducting. A subsequent 550°/10 hour oxygen anneal sharpens the transition.

During the present quarter the design of the furnace extension was completed, parts were fabricated, and construction was begun. The furnace extension is 3.3 meters long with five separately controllable zones with resistance heating. Provisions are made to allow atmosphere control independent of the main RTC furnace. Nextel woven ceramic fiber is again used to support the green clad fiber. In the high temperature RTC furnace, the Nextel carrier

belt is supported by the metal mesh conveyor belt. In the binder burnout extension, the Nextel belt is transported by drive rolls driven by the RTC belt drive mechanism. An important feature of the extension is a window to allow the fiber to be observed during binder burnout. This will prove invaluable to characterizing and troubleshooting the sintering process.

We anticipate that the furnace extension will be completed early in the next quarter. At that point the continuous fiber apparatus will consist of a 5.5-meter long furnace with eight controlled heating zones and two independent atmosphere zones, with payout and takeup spoolers capable of handling up to four individual filaments. This will be capable of producing four wires, each about 20-50 meters long per shift.
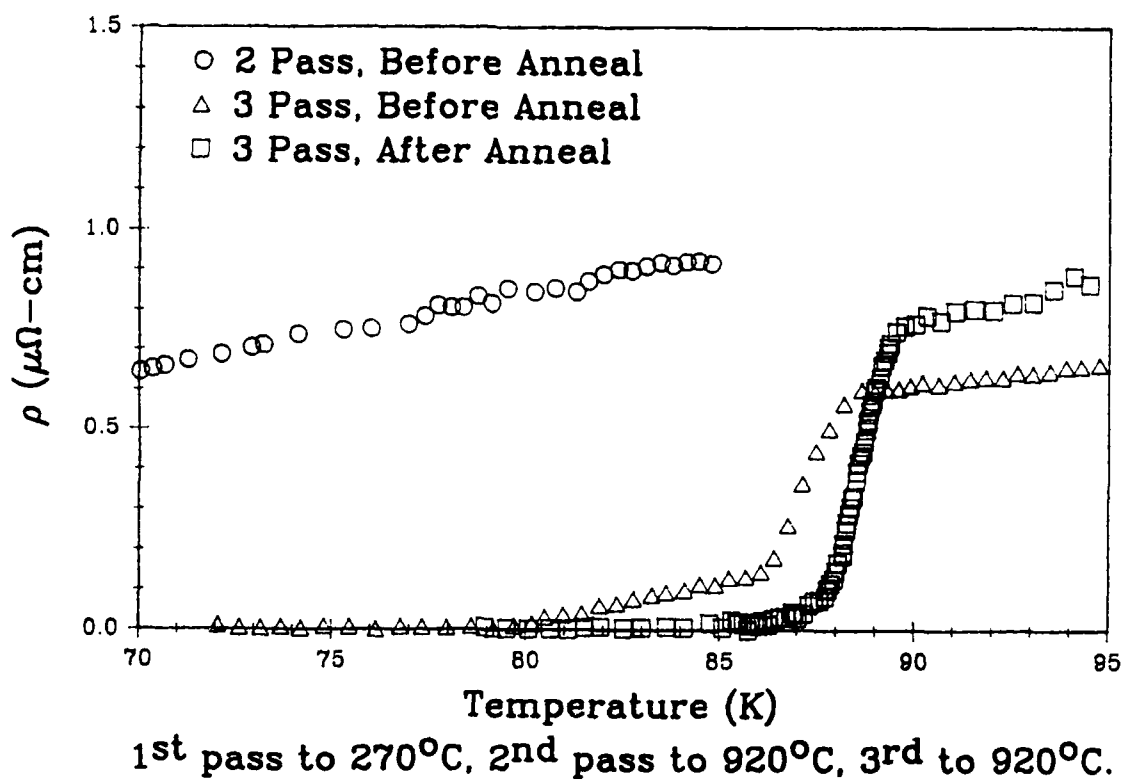
Figure 2.3.9   Resistivity vs. Temperature for Continuously Sintered Wire

2.4 Electrical Characterization

The majority of the effort in electrical characterization was the determination of self field transport critical current densities in support of the wire development effort, involving about 300 measurements. The notable results have been presented in the previous sections. Magnetic susceptibility measurements were used more commonly, and were correlated with transport data.

2.4.1 Measurement Technique

Transport measurements were conducted with the same method as previously reported. The specimen mounting and electroding procedure was again improved, however. Previously, specimens were mounted on a substrate with printed metal lines. Silver paint was used to fix the specimens and make electrical connection to the clad wire (or to fired-on silver contact pads on bare filaments). With this method the specimen was frequently damaged during cooling, apparently due to thermal expansion mismatch. We were unable to handle more porous and fragile specimens. We have overcome the thermal mismatch problem by suspending the specimen from free-standing copper lead wires, rather than fixing the specimen rigidly to a substrate. Fixtures have been made with four 5-mil copper wires attached to a connector. Specimens are placed on the wire and attached with silver paint, with voltage tap separation of 15-20 mm. This essentially eliminated our problem with breaking standard specimens, and allowed us to measure smaller and more fragile specimens.

Contacts to metal clad co-fired wires are simply made with commercial silver paint, and seem entirely satisfactory. Contacting bare fibers is done by applying painting silver pads to sintered filaments, which are subsequently re-fired to mature the silver pad. Some difficulty was encountered with this

procedure. We had previously obtained good results with a aqueous silver paint, re-fired during the 550°C oxygen anneal. Recently, however, this proved to be inconsistent. Unfortunately, it was not immediately obvious that the contacts were faulty, because the problem manifested itself as artificially low J_c values. Needless to say, this was alarming. The problem was solved by replacing the unreliable aqueous silver paint with a non-aqueous grade, and firing the contact pads in the RTC rather than during the oxygen anneal.

Figure 2.4.1 illustrates the E-J characteristics of good examples of the co-fired wire and bare Y-123 filaments, respectively. The current density in the clad wire is calculated on the cross-sectional area of the Y-123 core, rather than the net wire diameter. These represent the best performance to date on materials sintered as meter-long specimens. The difference in the E-J curves in the flux-flow region beyond the critical current density is related to current sharing in the silver cladding of the wire.

2.4.2 Critical Current Density in Applied Magnetic Field

Magnetic field measurements are routinely done on clad wire and bare filament to supplement the self field data. Standard practice is to determine J_c at 100 G for all specimens with a self-field value above $1000A/cm^2$. The full $J_c(B)$ characteristics is determined for selected specimens. Figure 2.4.2 and 2.4.3 are examples of a recent clad wire and bare filament. For the bare filament, critical current density drops rapidly from the $2200A/cm^2$ value at self field to about $10A/cm^2$ at 100G, then gradually drops to $5A/cm^2$ at 1000G. This value is still above the lower limit of measurable values for our apparatus.

Figure 2.4.4 displays some of the 100G measurements, showing the J_c at 100G as a function of the self field value. As expected , there is some correlation, but the scatter indicates that the shape of the $J_c(B)$ curve is variable for these specimens. The best specimens can carry about 22A/cm^2 at 100G.

2.4.3 Magnetic Susceptibility

Magnetic susceptibility data on our sintered filaments were obtained at Lake Shore Cryotronics using a Model 7000-1 AC Susceptometer.[3] The specimen is a single filament mounted coaxial with the magnetic field. Volume susceptibility at 200 Hz is calculated on a sample volume of 0.1 mm^3 (corresponding to a sample mass of 0.6 mg). Typically the measurements are done a 1G, although larger specimens give measurable signals at 0.1G. Figure 2.4.5 displays the susceptibility vs. temperature for 60 volume percent filaments sintered at temperatures between 875 and 996°C. Specimens sintered at 875°C have essentially no diamagnetic response down to 60K, which is consistent with poorly sintered material. The 900°C filaments are similar, with a very gradual buildup of diamagnetism below 75K. Filaments sintered at higher temperature all display on onset at 90K, with midpoint transition around 83K. Below this temperature the susceptibility curves diverge. Some of the difference might be attributed to specimen misalignment affecting the demagnetization factor, which could account for up to 10% variation in the calculated volume susceptibility, which is similar to the variability. Some of the difference reflects broadening

---

[3]. This instrument has been ordered and delivery is expected in February 1990.

of the transition due weak link effects in the 1 G magnetic field, since similar data taken at 0.1 G have sharper transitions. This will be examined in detail as more data is available.

The present data show no clear correlation between the self-field transport J_c and the real volume susceptibility. Figure 2.4.6 shows the real volume susceptibility (200HZ, 1G) at 74K and 60K plotted against J_c. Except for the lowest values, which are barely superconducting, the susceptibility values cluster around 0.8, while the weak-link critical current ranges between $250 \text{-} 2500 A/cm^2$. The real susceptibility, related to the Meissner effect, reflects the bulk quality of the superconductor, while the transport data are sensitive to interfacial weak link effects.

Initial characterization data is available for the "124" filaments made from the Y-123 + 10%CuO fibers. Recall that these fibers were presintered at 915°C, annealed 12 days at 810°C to form a substantial fraction of Y-124, then slow cooled in oxygen. There is no hint of a transition at 90K, so that little or no Y-123 is active. The peak of the imaginary susceptibility indicates a critical temperature of 77K, consistent with the Y-124 phase.

2.4.4 Splicing of Wire

Preliminary work has begun on the electrical resistance of splices in the silver clad wire. Two splicing techniques are under development. Finished wire, which has completed all anneals, will be spliced by a conventional solder lap joint. In-process wire, which must be subsequently sintered or annealed, will be spliced with a silver splicing sleeve made with the cladding suspension. Experiments are underway to characterize the electrical properties of these splices, but no reliable results are available at this time.
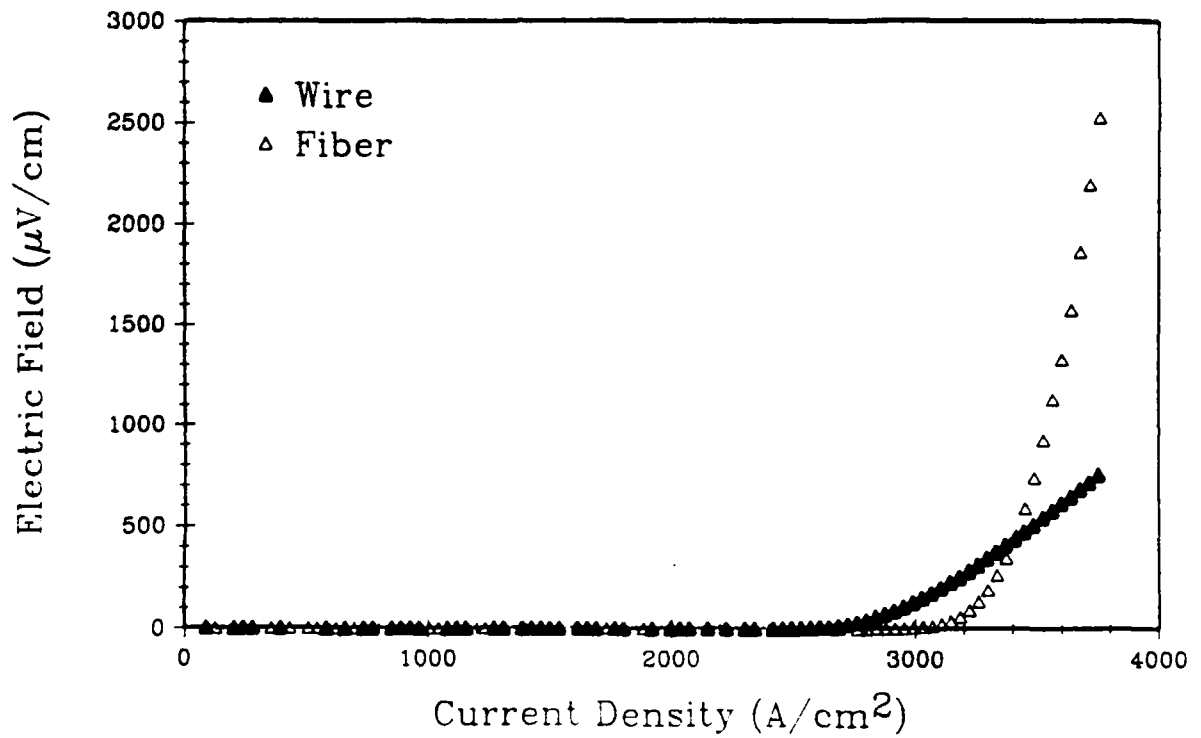
Figure 2.4.1   Electric Field vs. Current Density at 77K

in Self Field for Bare Fil;ment and Clad
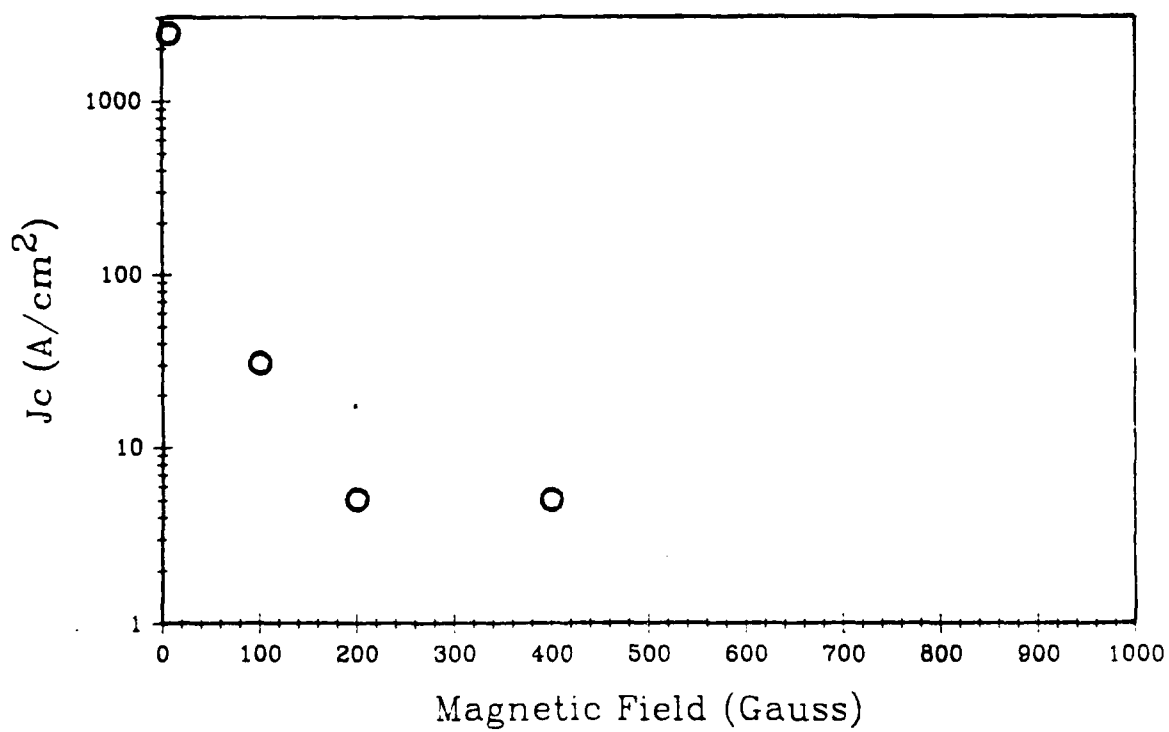
Wire

Figure 2.4.2   Critical Current Density vs. Magnetic
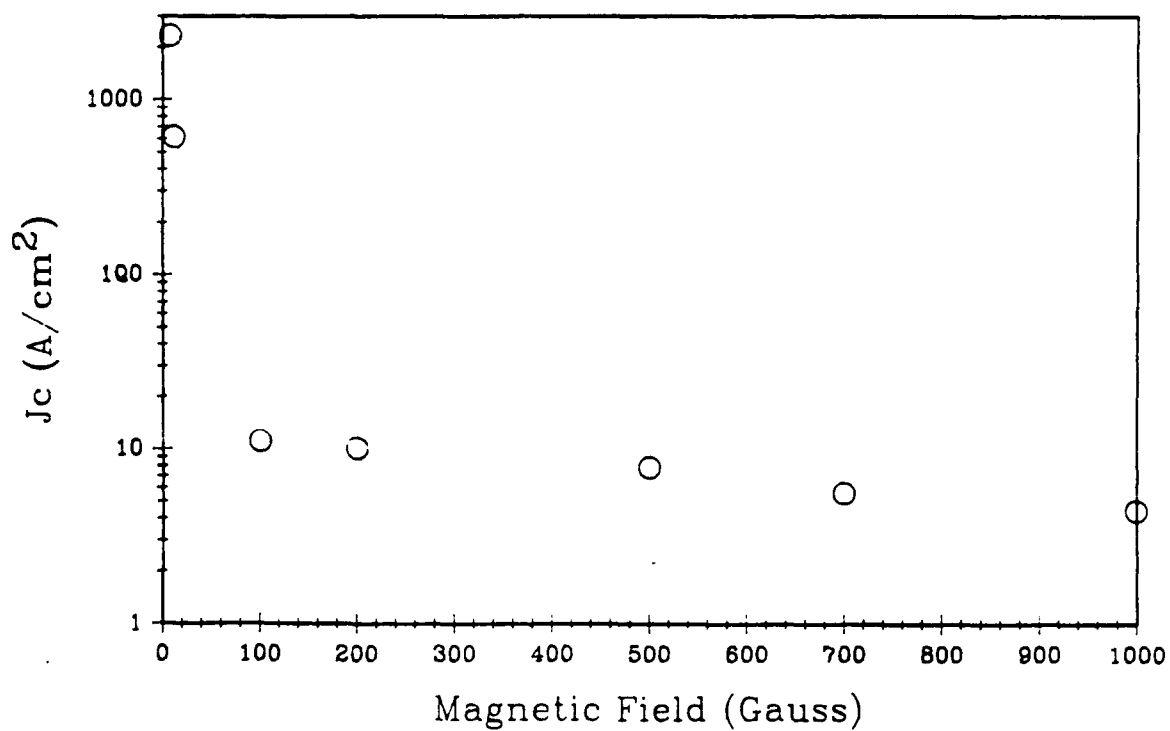   Field for Clad Wire at 77K

Figure 2.4.3   Critical Current Density vs. Magnetic
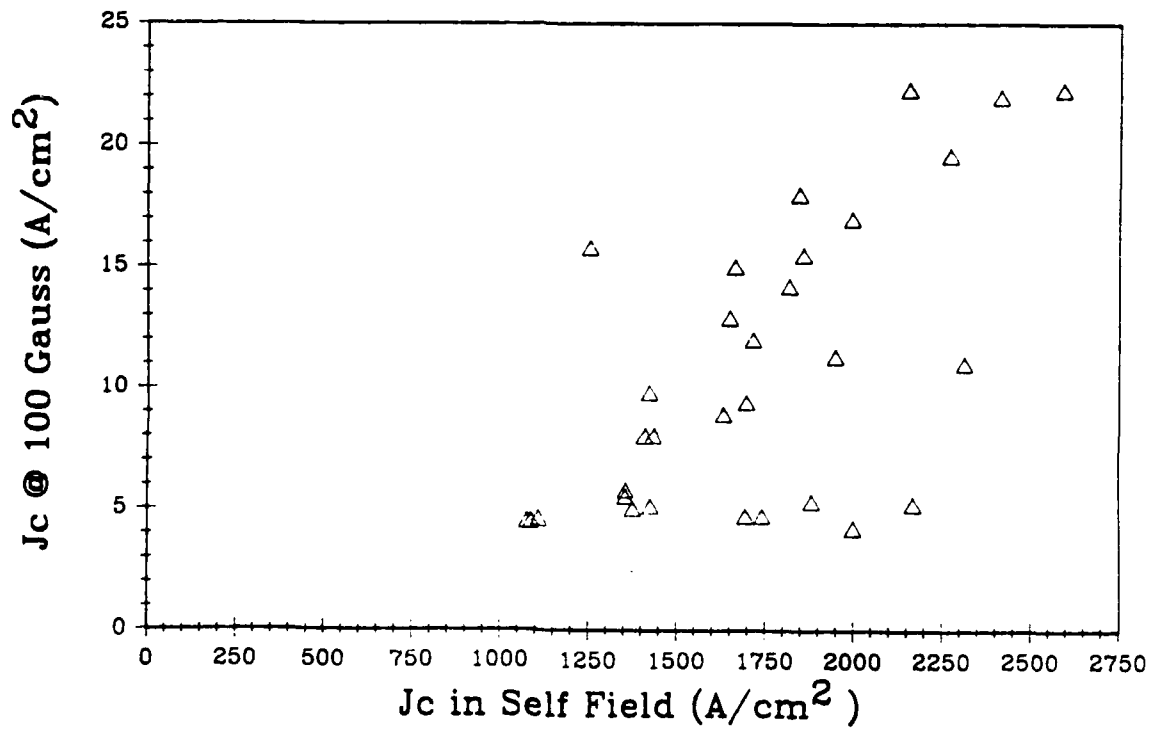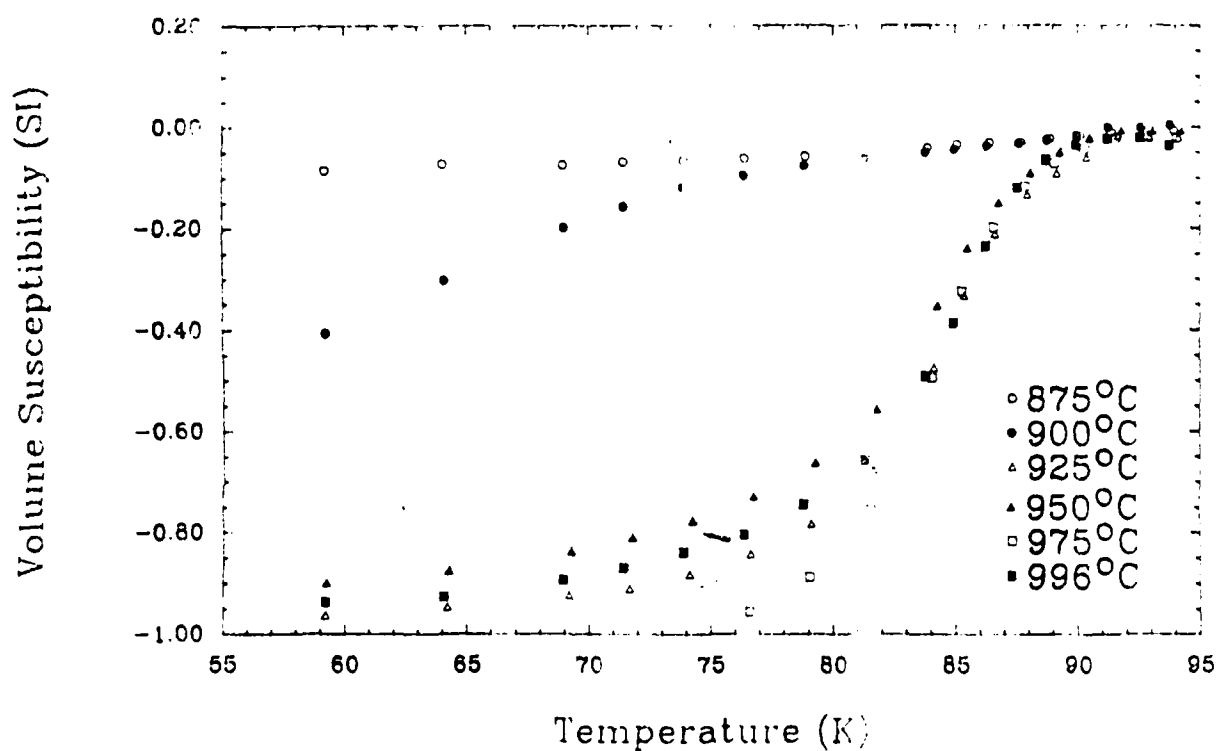
Field at 77K for Bare Y-123 Filament

Figure 2.4.4   Critical Current Density at 100 G vs. the Self-Field Value

X'(T) of 60 Vol% Fibers at 80 A/m, 200 Hz, $10^{-10}m^3$.

Figure 2.4.5   Magnetic Susceptibility as a Function of

Temperature for Sintered Filament from
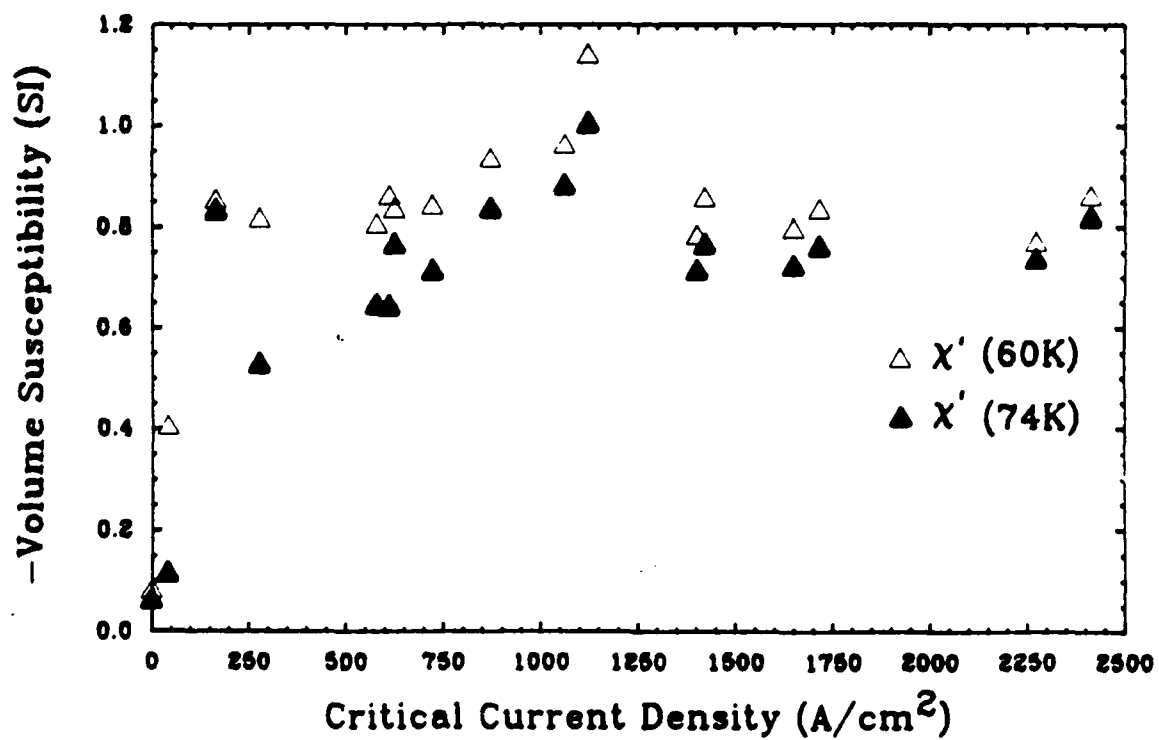
60 vol% Y-123 Fiber

Figure 2.4.6   Magnetic Susceptibility at 60K and 74K

versus 77K Self Field Critical

Current Density

2.5   Melt Processing of HTSC Wires

It is obvious that the electrical performance of sintered Y-123 wire is inadequate for practical HTSC motors or similar applications. During this quarter steps were taken to reorient the program to incorporate a melt texturing step compatible with wire manufacture. Our efforts involve continuing interaction with David Ginley at Sandia National Laboratory on rapid thermal processing (RTP), promising a very rapid production rate, and new activities involving directional solidification.

2.5.1 Directional Solidification of Wire

Directional solidification work is just now getting underway, involving internal effort at CPS and new external efforts at Arthur D. Little (ADL) and Oak Ridge National Laboratory (ORNL). These efforts will be closely coordinated and mutually supportive, aimed at defining the solidification behavior as a function of composition, temperature, gradient, and solidification rate. The ADL work, funded as a new subcontract commencing during the next quarter, will apply their technique of laser float zone crystal growth to prepare 10-20 cm long directionally solidified specimens. The ORNL program will be organized as a HTSC Superconductivity Pilot Center contract, supported with a combination of DOE funding and funds from this contract. The ORNL team will focus on solidification fundamentals, characterization, and arc-image experiments. The internal effort is aimed at conducting a directional solidification of the Y-123 conducted by zone melting the ceramic inside a sintered Ag-Pd clad wire. The approach is similar to work reported by Okada at Hitachi[5] and Yanagisawa at Asahi[6]. These activities are scheduled to be underway before the end or the next quarter.

2.5.2 Rapid Thermal Processing of Wire

Rapid Thermal Processing (RTP) of wire is being investigated in collaboration with D.S. Ginley et al. at Sandia National Laboratory. RTP experiments are conducted in an ADDEX-AET model R-1000 apparatus at Sandia. This unit is designed to accept 3-inch silicon wafers. We RTP anneal fibers by setting them on a nitrided silicon wafer. The ADDEX unit has a bank of halogen lamps which rapidly heat the chamber, reaching temperatures above 1000°C in 4 seconds. Typically the Y-123 fibers are held at 1000-1075°C for periods between 1 and 4 seconds, followed by a quench at cooling rates around 4°C/second. RTP anneals are conducted in rapidly flowing oxygen.

RTP experiments have been conducted on green and presintered fibers. In the case of green fibers, the polymer binder is first removed by a 600°C binder burnout treatment. Most work has been conducted on stoichiometric Y-123 and Y-123 doped with 1-10wt% copper oxide. Specimens consist of 15- and 225-micron fibers and braids.

Rapid thermal processing causes very rapid densification, as Y-123 filaments can reach densities estimated around 95% in only two seconds. Densification is accompanied by dramatic microstructural development associated with partial melting. In spite of the partial melting, XRD and TEM evidence indicate little second phase, so relatively little peritectic decomposition of Y-123 occurs.

After RTP treatment, fibers retain their round cross section. Indeed braided fibers retain the shaped and identity of the individual filaments. as illustrated in previous report.

The most remarkable property of the RTP filaments is that they are superconducting in the as-RTP'ed condition. RTP fibers have zero resistance at c. 90K and, under proper conditions, transport critical currents on the order of 1000 A/cm2. Collaborative RTP work is continuing, and will be reported fully in forthcoming publications.[7]

SECTION 3

HIGH TEMPERATURE SUPERCONDUCTOR

MOTOR DESIGN AND FABRICATION

ALAN CRAPO AND JERRY LLOYD

EMERSON MOTOR COMPANY

MOHAMED HILAL

UNIVERSITY OF WISCONSIN

3.1   Introduction

The superconductor motor work this quarter has been primarily concerned with brush testing and motor performance analysis. Motor construction is progressing, with most parts either completed or on order. We completed the testing of two brush grades and various slip ring materials. The brush system has been finalized. Finite element modeling of the flux and current distribution to calculate torque has improved ability to predict the motor performance. The characteristics of today's HTSC wire has been incorporated into the motor design. Motor performance has been calculated based on reduced magnetic field levels due to low J_c values in a magnetic field. The performance is summarized.

3.2   Homopolar Motor Construction

Motor construction is coming along well. All of the parts and equipment that are purchased or made outside are either here or are on order

and will be here soon. The rest of the parts are being made in our model shop. Some of the parts such as brushes, springs and the rotor were held up while the testing and analysis below was going on. Now that the tests are completed, the parts have been ordered.

A few minor design changes were made to some of the other parts to accommodate easy mounting, and improve reliability. The design of the stator pieces was modified to allow easy mounting to a support stand. The rotor design was modified to have helical grooves or threads to help the brush performance. This is discussed below in the brush testing section.

The HTSC wire is very fragile, and making the coils is very labor intensive. We've modified the coil/bobbin design so that a small fracture will not ruin an entire coil. The coil will be divided up as several individual coils that can be tested individually and connected in series or parallel combinations. In this way a damaged or weak section of wire can be bypassed and the coil will still be usable with reduced effective turns. The leads will be connected to terminals so the connections can be made outside the motor in a room temperature environment.

We are working with Phelps Dodge Corporation and University of Wisconsin on the insulation for the HTSC wire.

3.3   Brush Testing

3.3.1   Brush Friction

A major component of loss in our homopolar motor will be brush friction. We made some friction measurements in order to calculate the frictional coefficient between the brush and slip ring material. This test was done with the threaded steel slip ring and both brush materials.

Using a DC motor as a prime mover, we rotated the slip ring assembly at 800 RPM. We measured the difference in current draw of the DC motor when the brushes were loaded and unloaded. The following data was taken to calculate the friction:

Motor K_t = 60.9 oz-in/A.

Brush area = 0.310in x 0.625in = 0.19375 in^2 for each brush.

Brush force = 12.0 ounces per brush.

Slip ring radius = 0.625 inch

Change in current = 45mA. for 85% copper brush

42mA. for 65% copper brush

From these data we can calculate the friction torque to be 2.74 oz-in for the 85% copper brush and 2.56 oz-in for the 65% copper brush. The drag force per brush is then 2.19 ounce force for 85% copper and 2.05 ounce force for the 65% copper brush. With an applied spring force of 12.0 ounces on each brush, the pressure is 3.9 PSI, and the frictional coefficients are calculated as 0.18 and 0.17 for 85% and 65% copper brushes.

3.3.2 Voltage Drop tests

The best motor design from a magnetic point of view uses steel slip rings. We wanted to make sure the steel slip ring would work as well as copper and brass. We tested two brush grades on four slip ring surfaces to determine the best combination for the motor. Since the contact drop in the brush represents the largest component of loss, it is important to reduce it as much as possible. The two brush grades tested were 65% copper. and 85% copper mixed with graphite. We tested these brushes on slip rings made of copper, brass, smooth steel, and steel with threads. These tests were done both at room temperature and in liquid nitrogen at a speed of about 1900 RPM

on a 0.625 inch radius. The brush pressure was 3.9 PSI at room temperature in each case. The voltage drop across two brushes is series versus current density was recorded for each condition.

We had difficulty with the copper and brass slip rings at high current densities when submerged in liquid nitrogen in that there was some arcing and damage to the slip ring and brush. We did not attempt high current densities in room temperature air because of fear of overheating. We assumed that there would not be an overheating problem in liquid nitrogen. Whether or not the arcing was caused directly by heat is not clear, but arcing damage was significant.

The smooth steel slip ring did not have arcing problems but we found that as the brushes ran with current for very long (10-15 minutes), a high resistance film began to build up. The longer the brushes ran with current, the greater the resistance buildup. The data taken for the smooth steel slip ring was taken before much film buildup occurred. The copper, brass, and steel smooth slip rings each had problems.

We then found out that the correct way to use steel slip rings and not get the film build up was to put threads on the steel surface. The helical threads give a continuously changing edge between the copper and the steel. The threaded steel slip ring had no significant arcing, and no significant film buildup. The voltage drop characteristics were also pretty good. We used 16 threads per inch on the test slip ring. We have modified the rotor/slip ring design of the homopolar motor to also have 16 threads per inch.

The following table lists the results of the tests:

VOLTAGE DROPS

Brush %Cu	Slip Ring	Environment	Brush current density (A/in^2)				
			5.2	25.8	103	207	361
65	Copper	Room Air	.055	.21	.43		
65	Copper	Liquid Nitrogen	.09	.16	.32	.42	.49
65	Brass	Liquid Nitrogen	.29	.43	.73	.89	1.05
65	Smooth Steel	Liquid Nitrogen	.63	.75	.90	1.02	1.10
65	Threaded Steel	Room Air	.045	.18	.46		
65	Threaded Steel	Liquid Nitrogen	.46	.49	.55	.62	.65
85	Copper	Room Air	.015	.07	.23		
85	Copper	Liquid Nitrogen	.08	.21	.35	.41	.50
85	Brass	Room Air	.018	.057	.18		
85	Brass	Liquid Nitrogen			.29	.46	.60
85	Smooth Steel	Liquid Nitrogen	.18	.26	.34	.40	.48
85	Threaded Steel	Room Air	.006	.027	.10		
85	Threaded Steel	Liquid Nitrogen	.065	.15	.26	.33	.39

The data on the above table is shown graphically in figures 3.3.1 through 3.3.8. For each set of data points, a best statistical fit is calculated based on a power fit of the form $V = A*I^B$ where A and B are constants. The current, I, is shown as the current in the homopolar motor calculated from the above current densities. The film buildup on the steel slip rings is probably a factor in the shape of the curves. There may be some film or other effect caused by the liquid nitrogen. It's not clear if the fluid dynamics or the temperature is the main reason for the difference in shapes of the curves, but the intent of this program is not to do a thorough
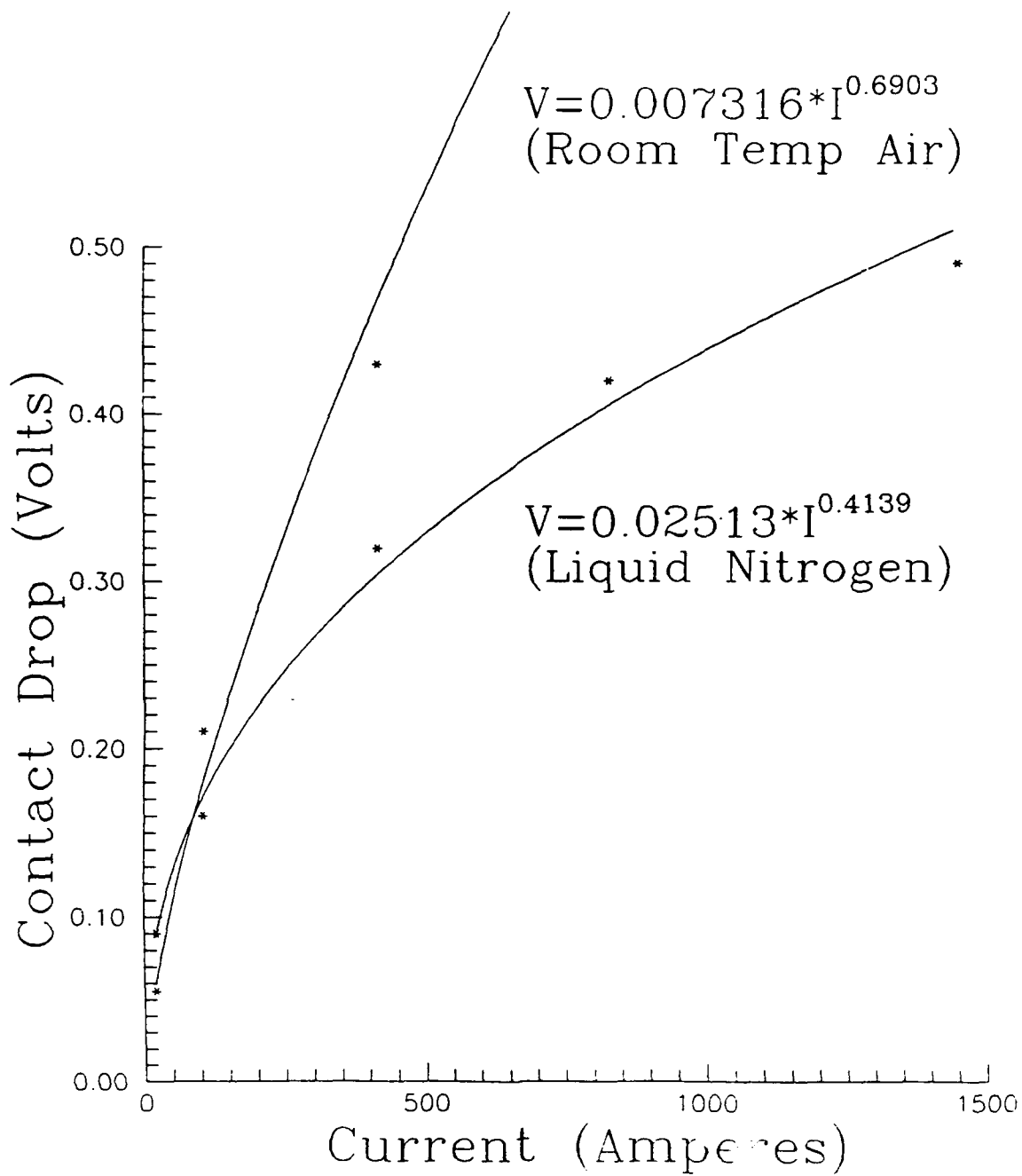
$V = 0.007316 * I^{0.6903}$
(Room Temp Air)

$V = 0.02513 * I^{0.4139}$
(Liquid Nitrogen)

Figure 3.3.1
65% Copper Brush
Copper Slip Ring

$$V = 0.1092 * I^{0.3110}$$
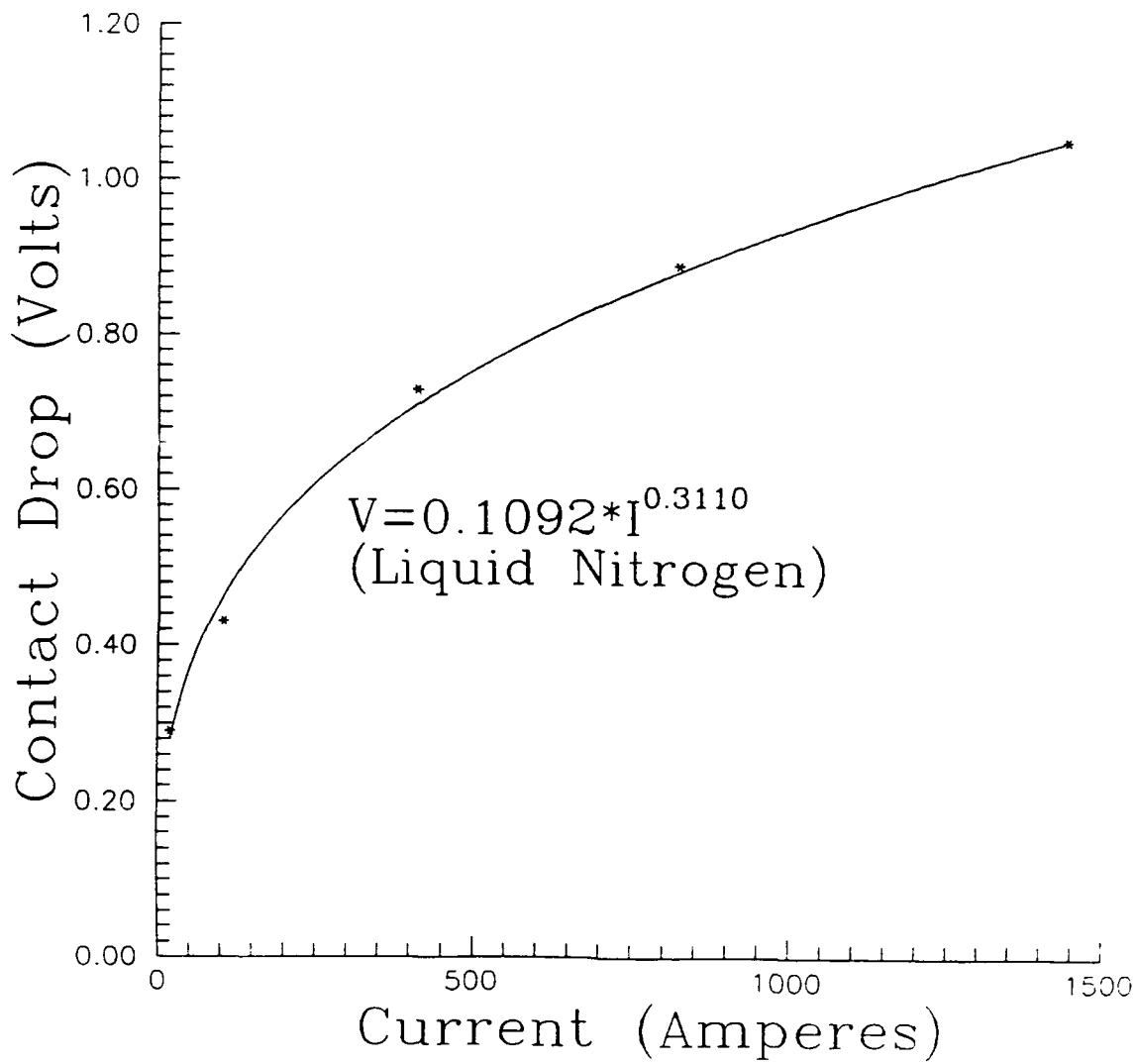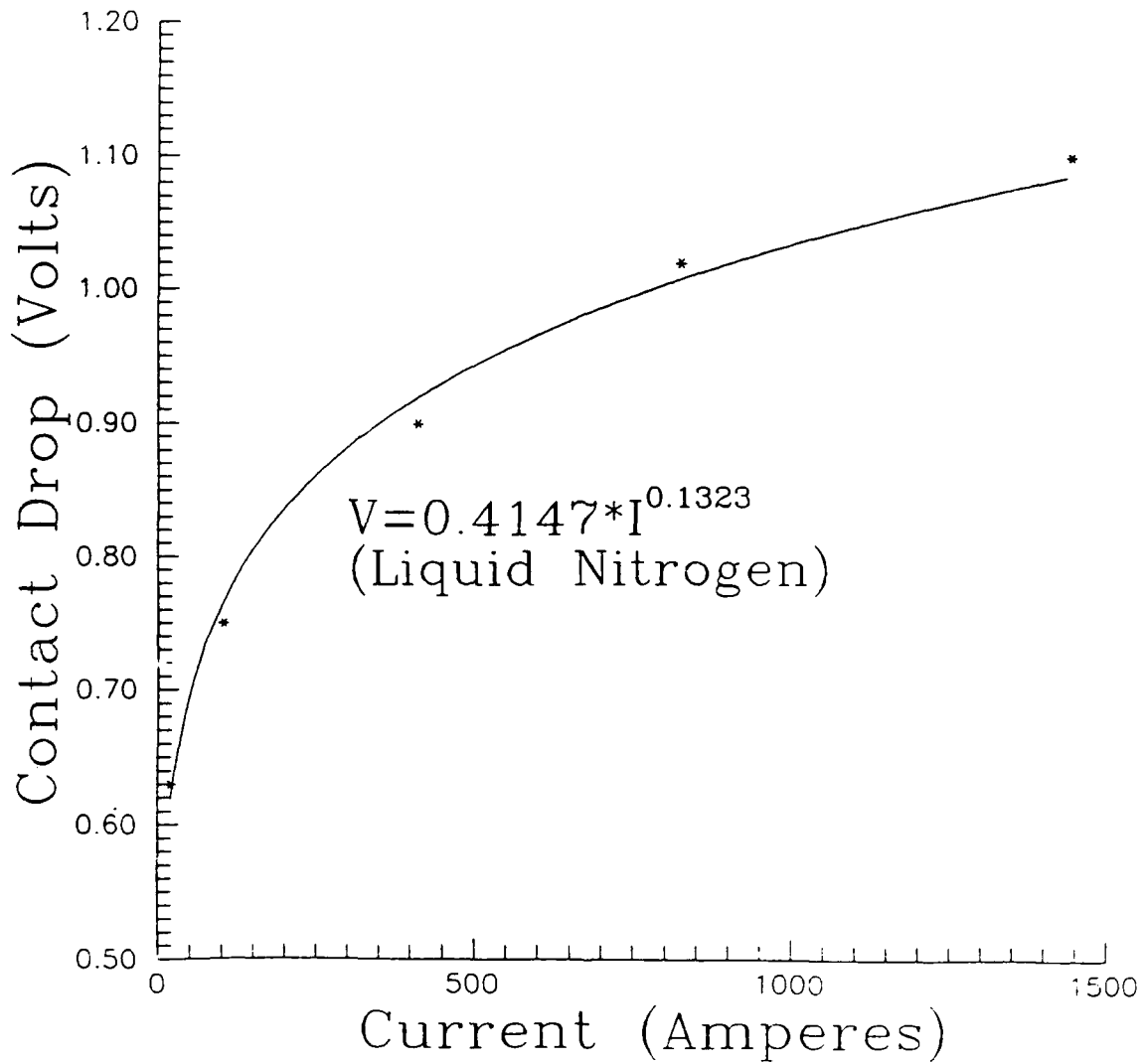(Liquid Nitrogen)

Figure 3.3.2
65% Copper Brush
Brass Slip Ring

Figure 3.3.3
65% Copper Brush
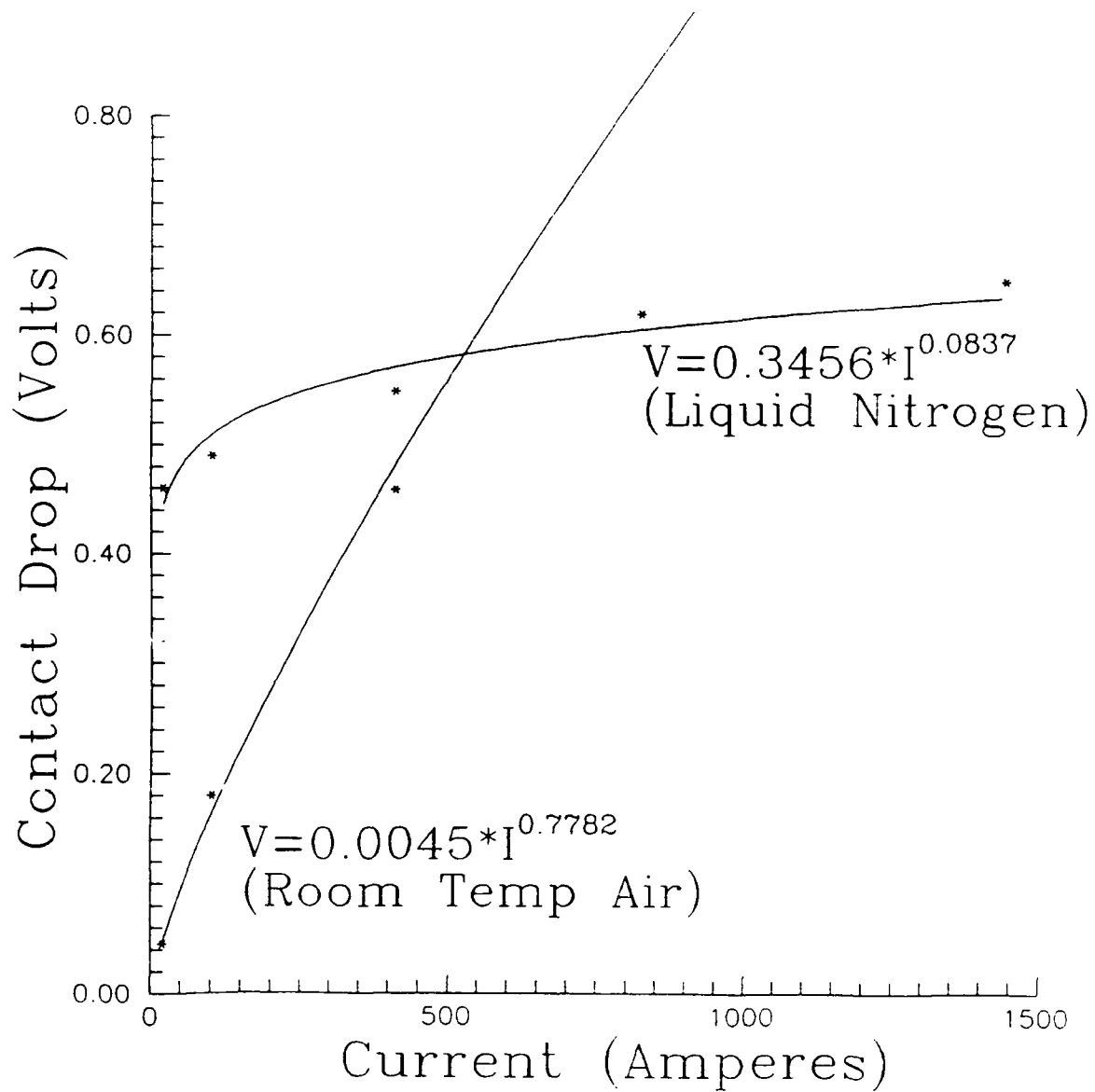Smooth Steel Slip Ring

Figure 3.3.4
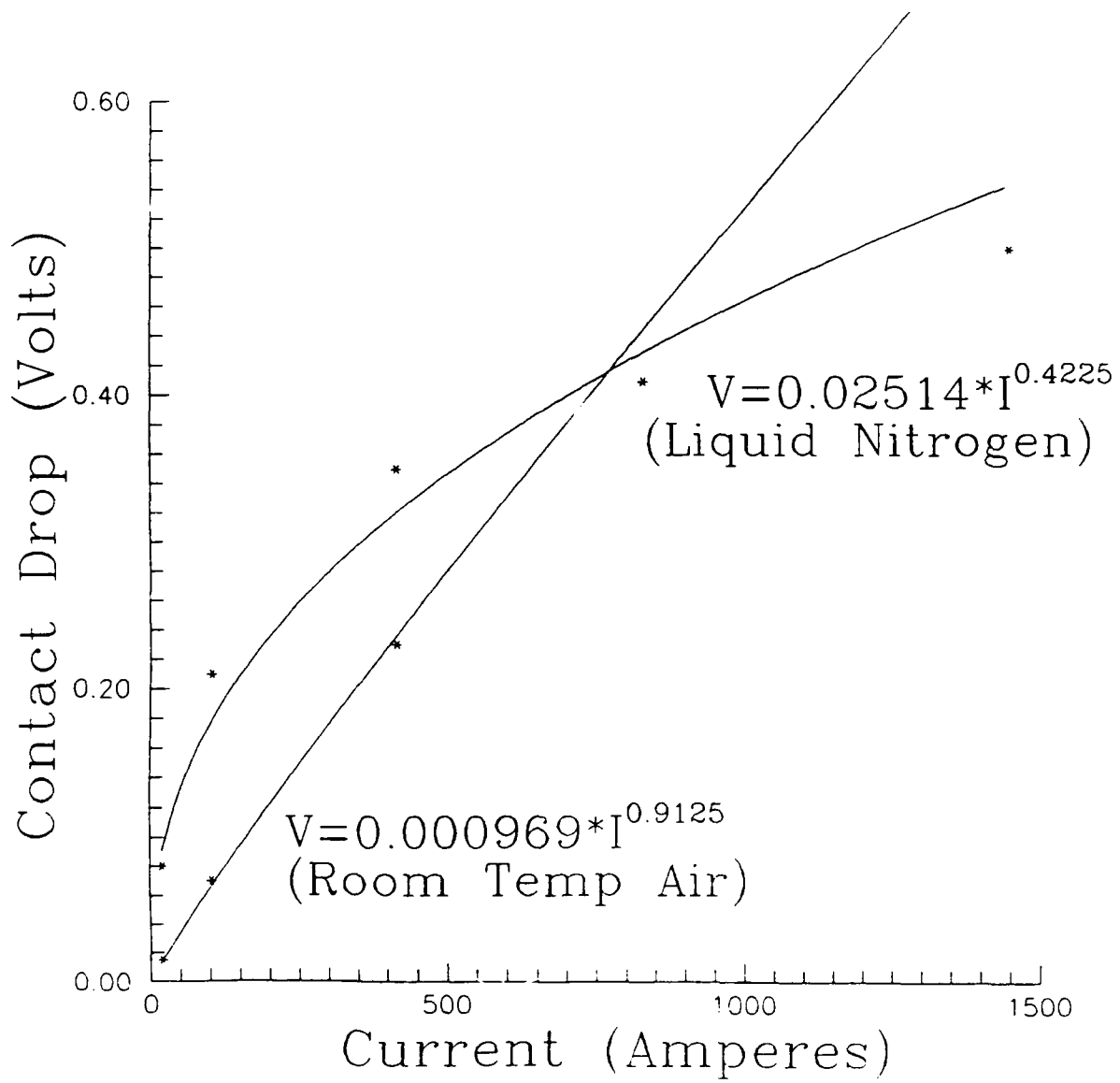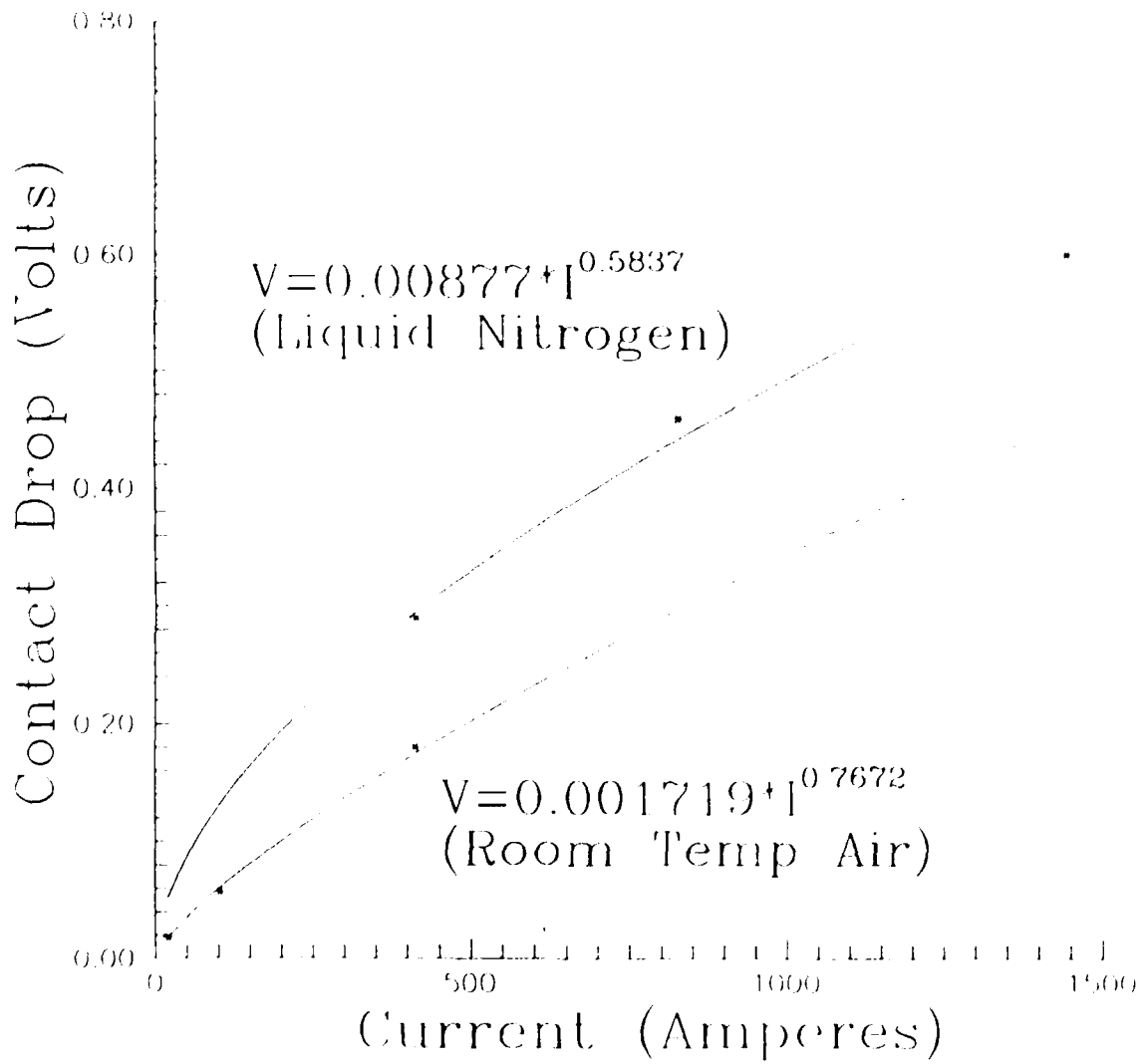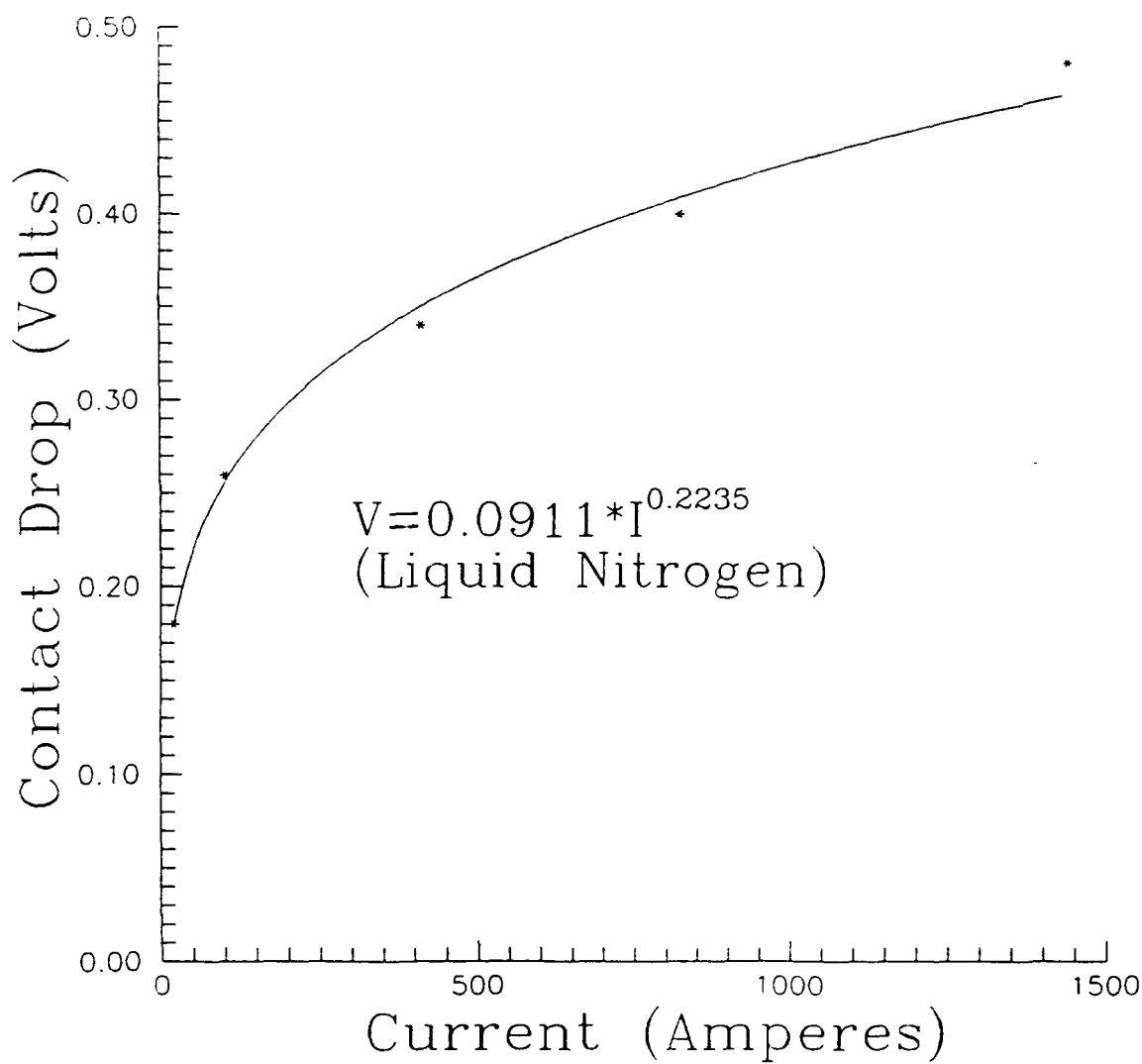65% Copper Brush
Steel Slip Ring
(16 Treads per inch)

$$V=0.02514*I^{0.4225}$$
(Liquid Nitrogen)

$$V=0.000969*I^{0.9125}$$
(Room Temp Air)

Figure 3.3.5
85% Copper Brush
Copper Slip Ring

Figure 3.3.6
85% Copper Brush
Brass Slip Ring

$$V = 0.0911 * I^{0.2235}$$
(Liquid Nitrogen)

Figure 3.3.7
85% Copper Brush
Smooth Steel Slip Ring

$$V=0.01945*I^{0.4217}$$
(Liquid Nitrogen)
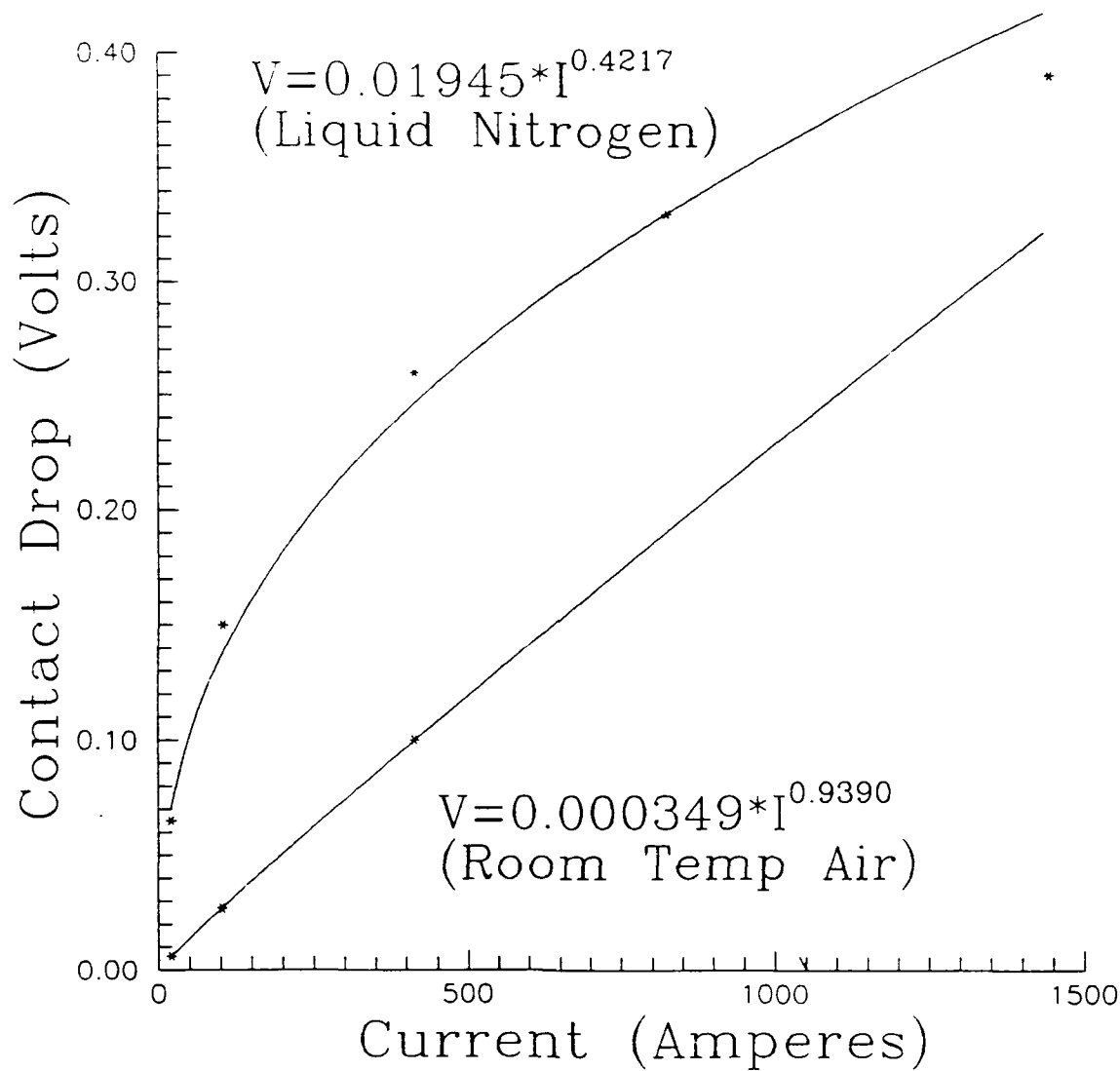
$$V=0.000349*I^{0.9390}$$
(Room Temp Air)

Figure 3.3.8
85% Copper Brush
Steel Slip Ring
(16 Treads per inch)

in depth study of brushes and slip rings, but to find a system that will work.

Additional brush testing that still needs to be done is to look at the effects of speed and brush pressure on the voltage drop so we can adjust the brush pressure to an optimum value.

3.4   Homopolar Motor Performance Calculations

3.4.1   Effects of J_c Reduced by Magnetic Field.

Our coil design is based on our wire performance goal of 1000 Amperes/cm^2 in a field of 100 Gauss or 0.01 Tesla. Wire built to date still does not reach this performance level. The present wire samples can carry 2600 Amperes/cm^2 in a zero Gauss field, but J_c is greatly reduced in the presence of a magnetic field. Figure 3.4.1 shows how J_c decreases as the field increases. The other two lines show the peak field produced at the coil as a function of the current in the coil for a 4600 turn and for a 9200 turn design. The line for 4600 turns intersects the wire line at a field of 26 Gauss and a J_c of 260 Amperes/cm^2. This means the motor would operate at a maximum of 26% of the designed field level. This can be improved by increasing the turns on the coil. The 9200 turn (doubled) design would operate at about 35% of the designed field level with a J_c of about 175 Amperes/cm^2. This is an improvement, but takes twice the length of wire. The additional turns would be very difficult to justify.

3.4.2   Torque, Power, and Efficiency

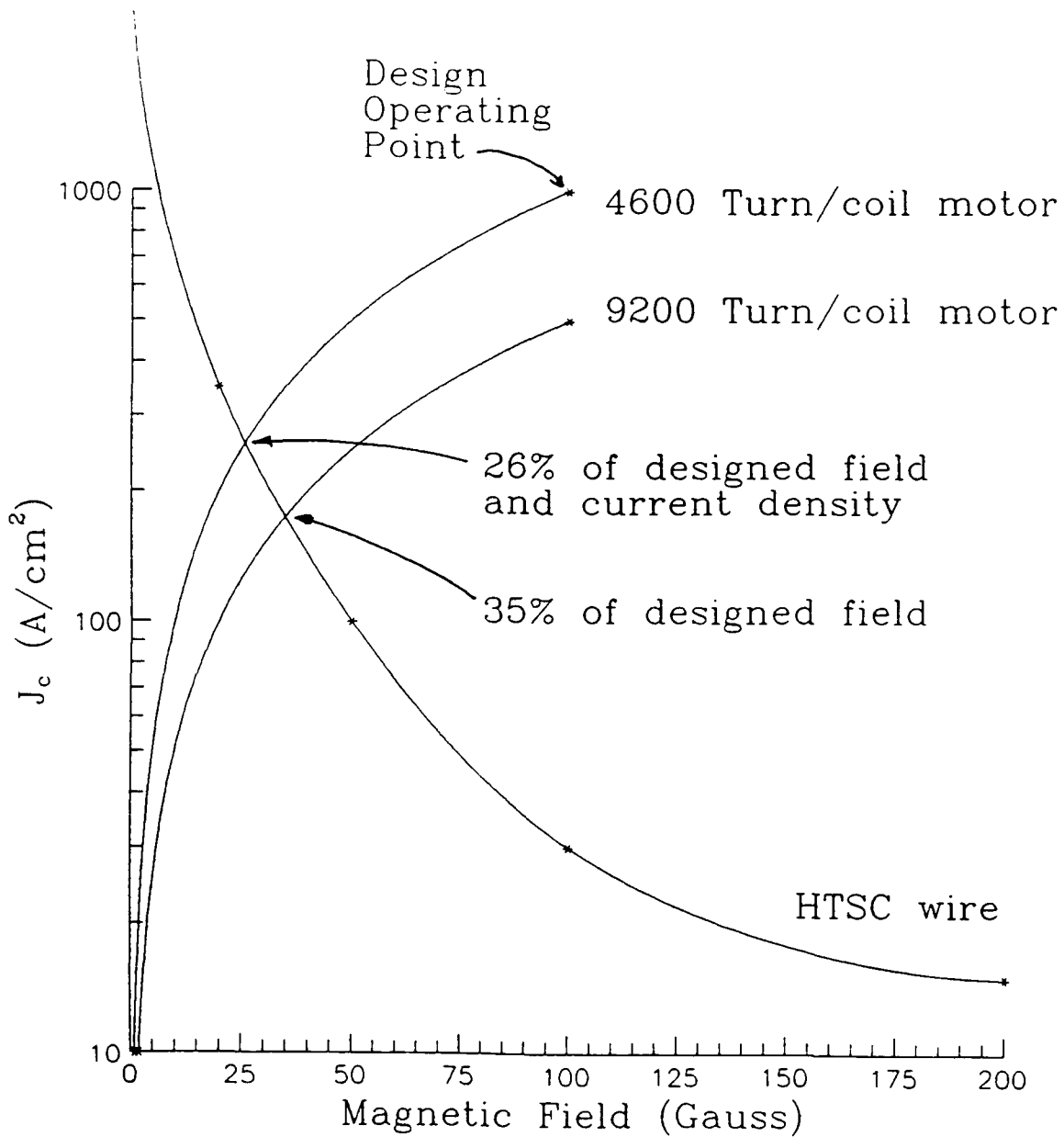In general, torque in a drum type homopolar DC motor can be expressed as:

Figure 3.4.1 Current density Vs. magnetic field for HTSC wire and for motor coils.

Torque = Flux Density(B) X Current(I) · (Length of conductor path in

B field) · (Radius)

or

Torque = B X I · l · r.

But B and I have non uniform distributions, and l and r vary. Finite element modeling was used to calculate B, I, l, and r throughout the active volume of the motor and calculate the torque. Figure 3.4.2 is the flux plot showing the distribution of B, based on the designed 575 Ampere turns per coil, as a function of r (radial position) and z (axial position). Figure 3.4.3 is a current contour map showing the current distribution as a function of r and z. The torque produced in each element was summed to give the entire motor torque:

Torque = 3.837 Nm with 1000 Amperes of current.

This is 95% of the torque calculated if we assume all of the current stays .i surface of the rotor.

To calculate the actual shaft torque, the friction torque needs to be subtracted from the electrical torque. Friction torque comes mostly from the brushes and varies linearly with brush pressure. The input voltage required is the back EMF plus the voltage drops across the brushes. We can neglect other losses for our first order calculations. The back Emf varies with speed and the flux of the motor. The voltage drops in the brush for a given brush and slip ring material vary with current in a nonlinear power relationship shown previously, and brush pressure. The brush manufacturers suggest that the voltage drop varies with the brush pressure to about 0.6 power. The torque calculations shown above assume the field coils have the designed 575 Ampere turns on each coil, and there is no friction. In the actual motor, we
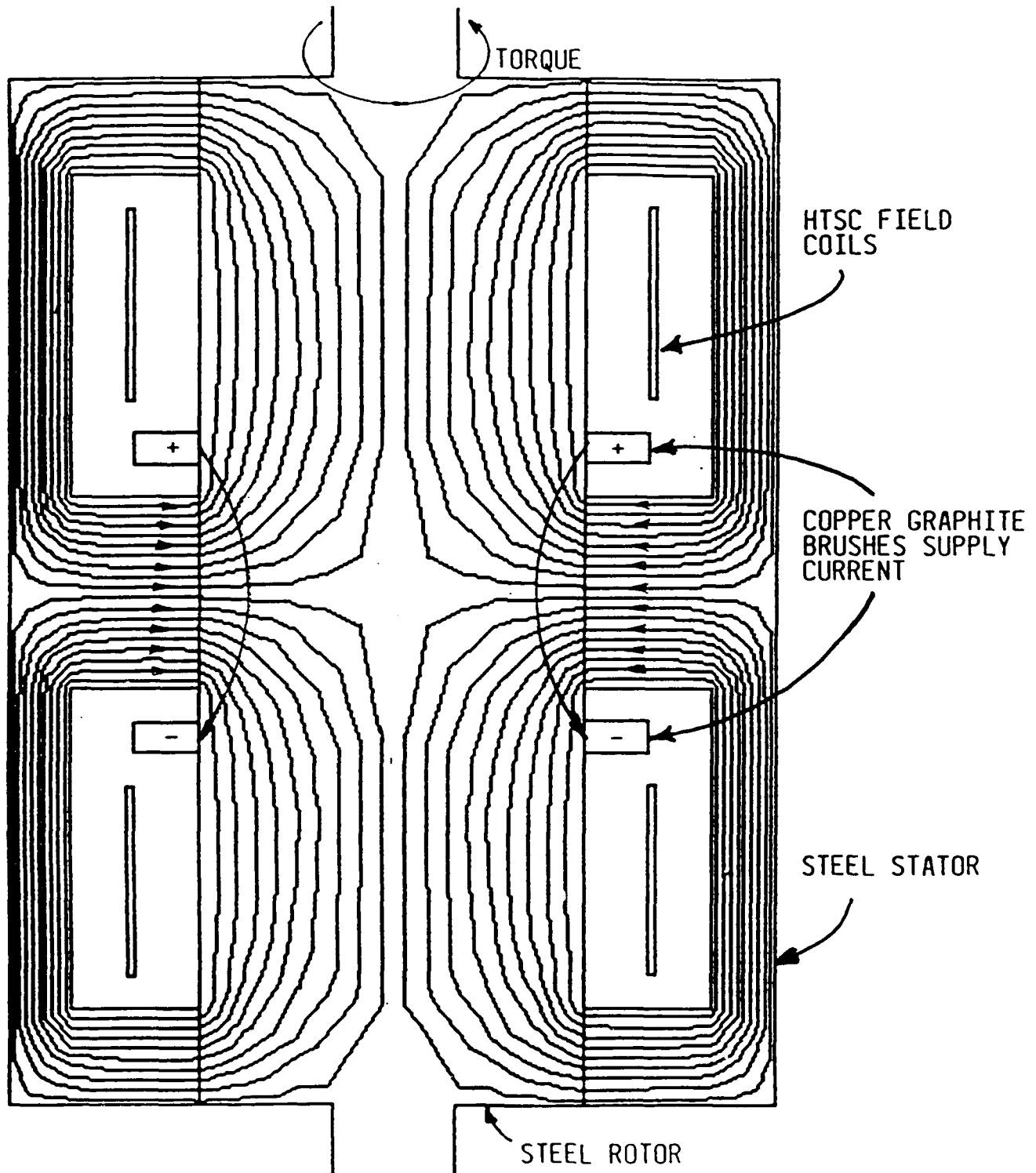
STEEL CORE HOMOPOLAR
MOTOR FLUX PLOT

TORQUE

HTSC FIELD
COILS

COPPER GRAPHITE
BRUSHES SUPPLY
CURRENT

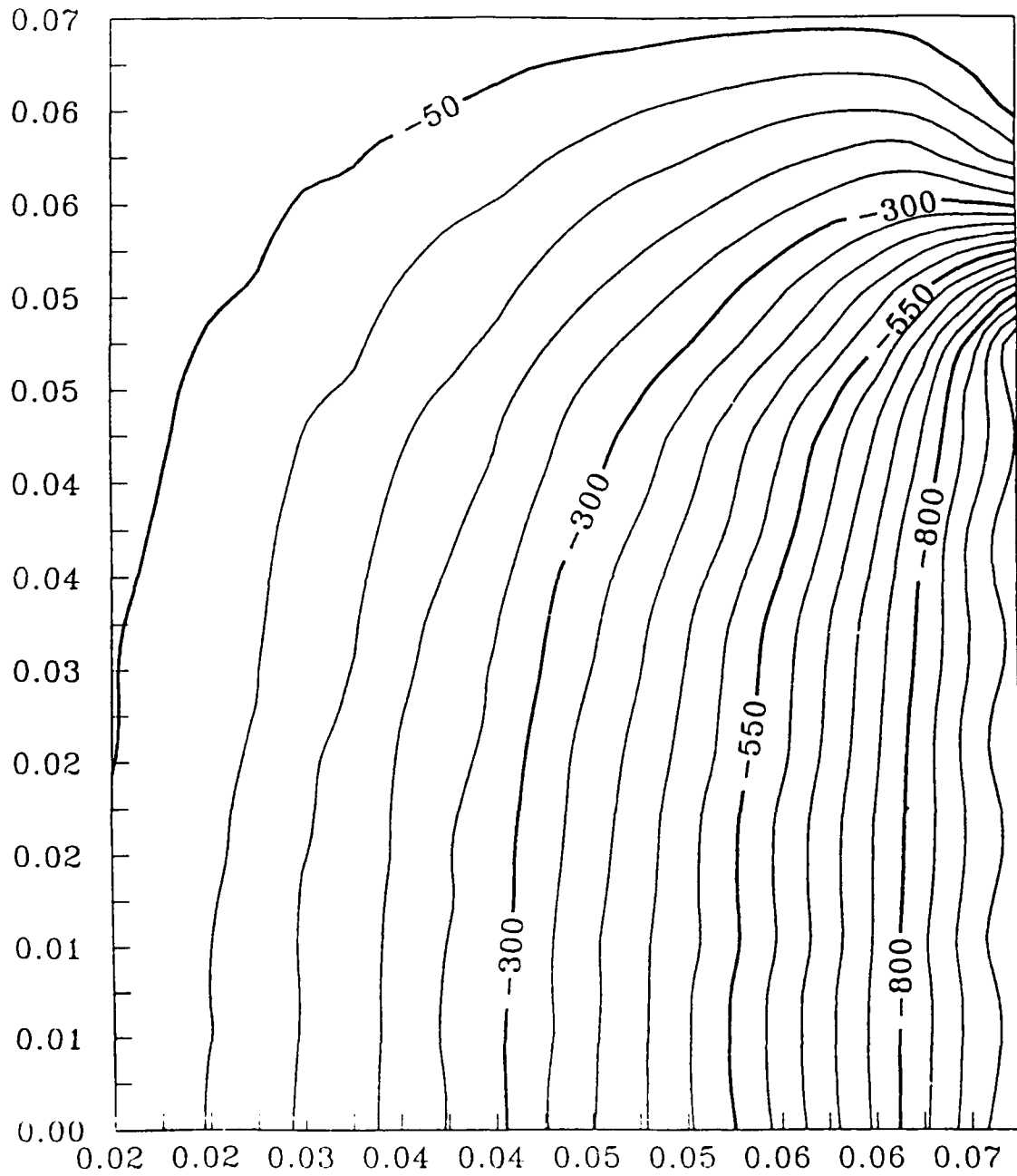STEEL STATOR

STEEL ROTOR

Figure 3.4.2

CURRENT CONTOUR

FIGURE 3.4.3

will not be able to get full design current in the coils due to the limitation

of J_c as described earlier. The following equations which describe the motor

performance include the field level as a percentage of the original design.

Electrical torque = 3.837Nm x (percent field/100) x (current/1000)

Friction Torque = 0.488Nm x (Brush pressure in psi)

Shaft torque = Electrical torque - Friction torque

Mechanical power = Torque x Speed(radians per second)

Back EMF Voltage = 0.000402 x speed(RPM) x (percent field/100)

Voltage drop in Brushes =

0.01945 x $Current^{0.4217}$ x (3.9 x Brush pressure in psi)$^{0.6}$

Input voltage = Voltage drop + Back EMF

Electrical power = Voltage x Current.

Losses = Friction power + Brush losses

Figure 3.4.4 shows the results of these performance equations plotted

against brush pressure for the field at the original design level of 575

Ampere turns per coil. The losses are at their minimum value between 1.5 and

2.0 psi brush pressure. Figures 3.4.5 through 3.4.8 show the same curves for

field strengths of 50%, 35%, 26%, and 20% of the designed level. As the field

is weakened, the motor is capable of producing less and less torque. As

previously shown, with the wire in its current state of development, we should

be able to get 26% of designed field from the coils. Conservatively, we can

expect 20%. Figure 3.4.9 shows the curves with 20% field but the current

increased to 1500 Amperes. The performance is greatly improved.

The curves suggest the optimum brush pressure to be lower than the 2

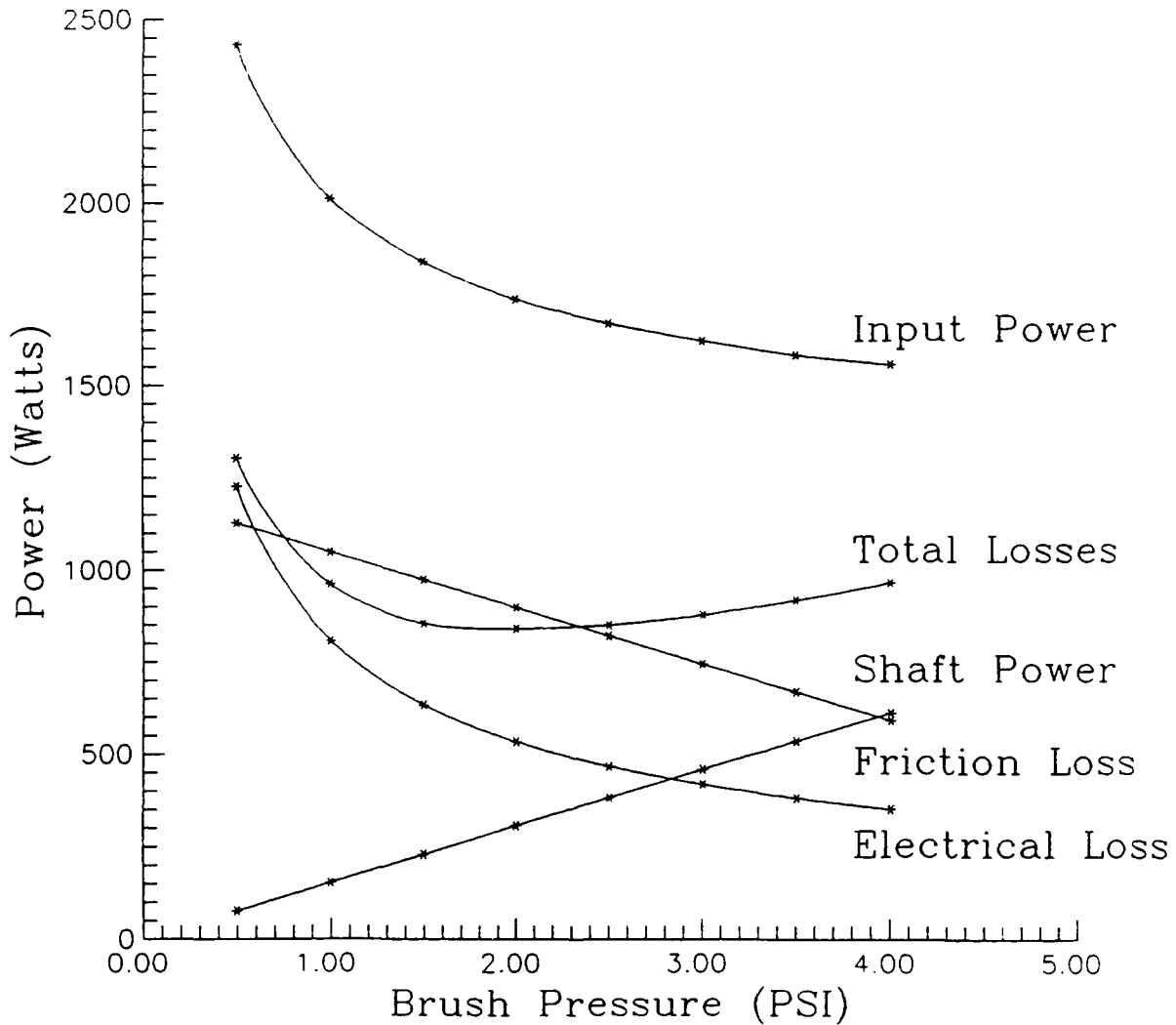to 4 psi recommended by the brush manufacturer. We will have different

Figure 3.4.4   Motor Power and Losses Vs. Brush
Pressure for 100% Field Coil Ampere Turns.
Speed is 3000 RPM.   Current is 1000 Amperes.

Figure 3.4.5 Motor Power and Losses Vs. Brush
Pressure for 50% Field Coil Ampere Turns.
Speed is 3000 RPM. Current is 1000 Amperes

Figure 3.4.6   Motor Power and Losses Vs. Brush
Pressure for 35% Field Coil Ampere Turns.
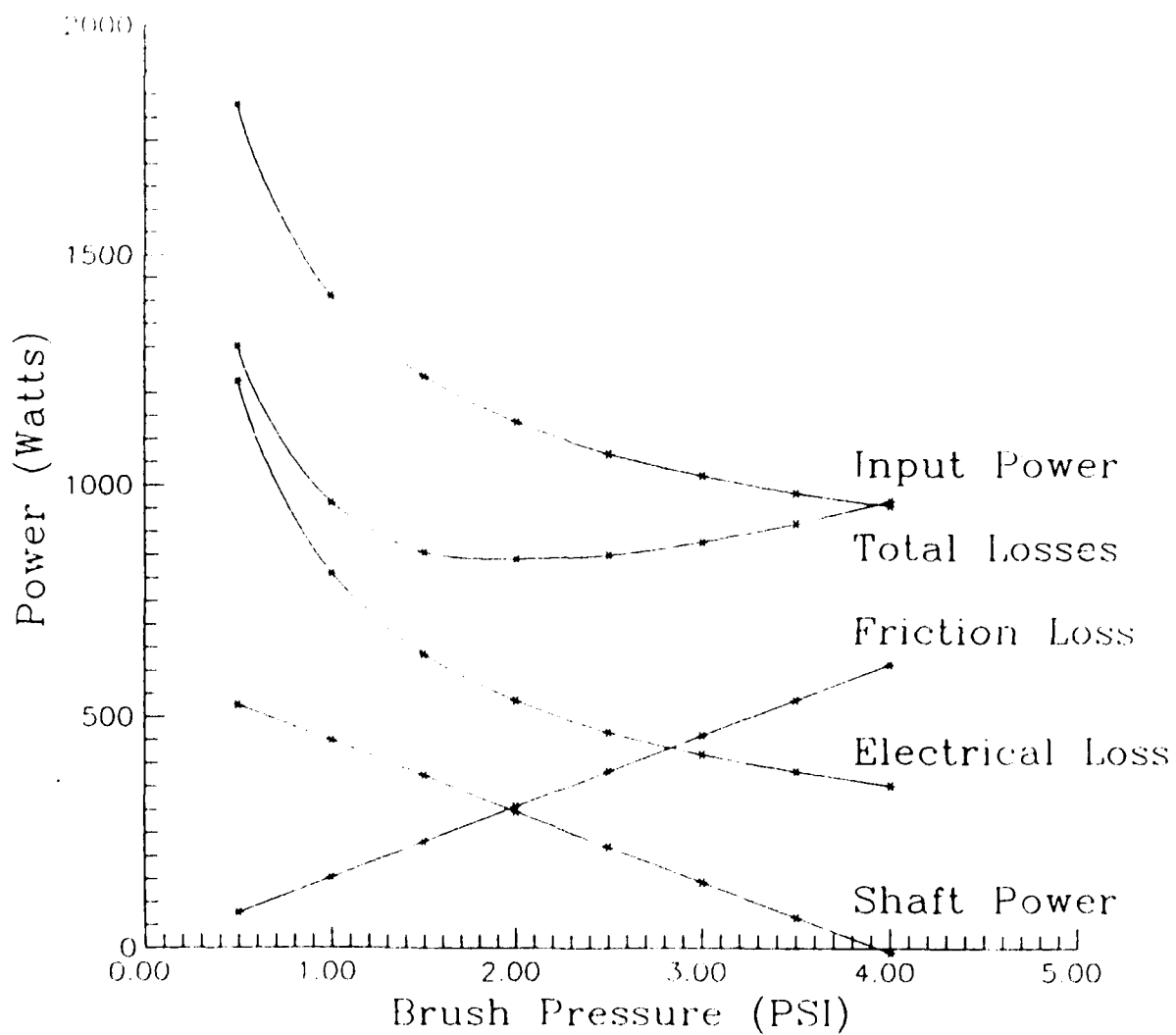Speed is 3000 RPM.   Current is 1000 Amperes.

Figure 3.4.7   Motor Power and Losses Vs. Brush
Pressure for 26% Field Coil Ampere Turns.
Speed is 3000 RPM.   Current is 1000 Amperes.

Figure 3.4.8   Motor Power and Losses Vs. Brush Pressure for 20% Field Coil Ampere Turns. Speed is 3000 RPM.   Current is 1000 Amperes.
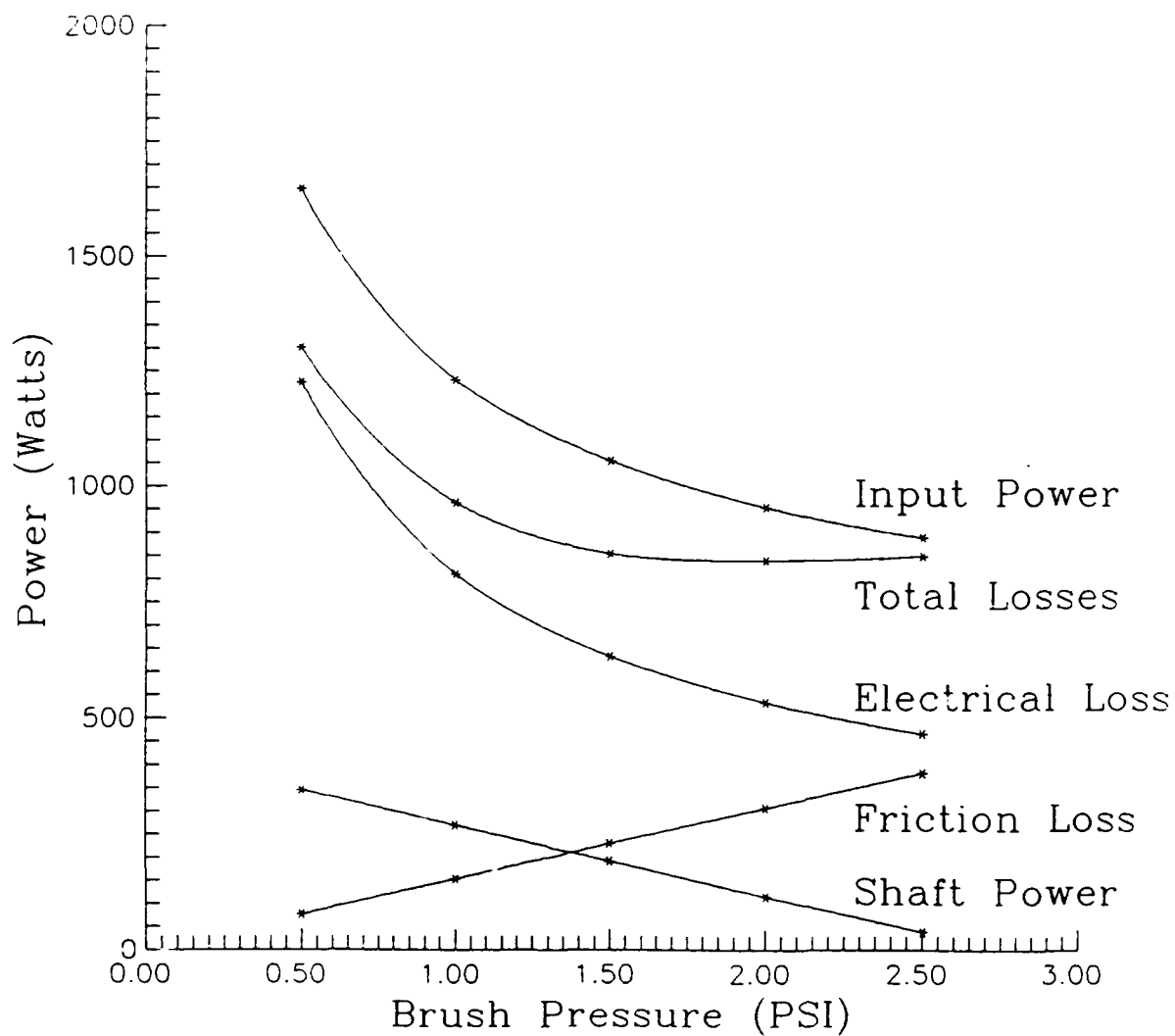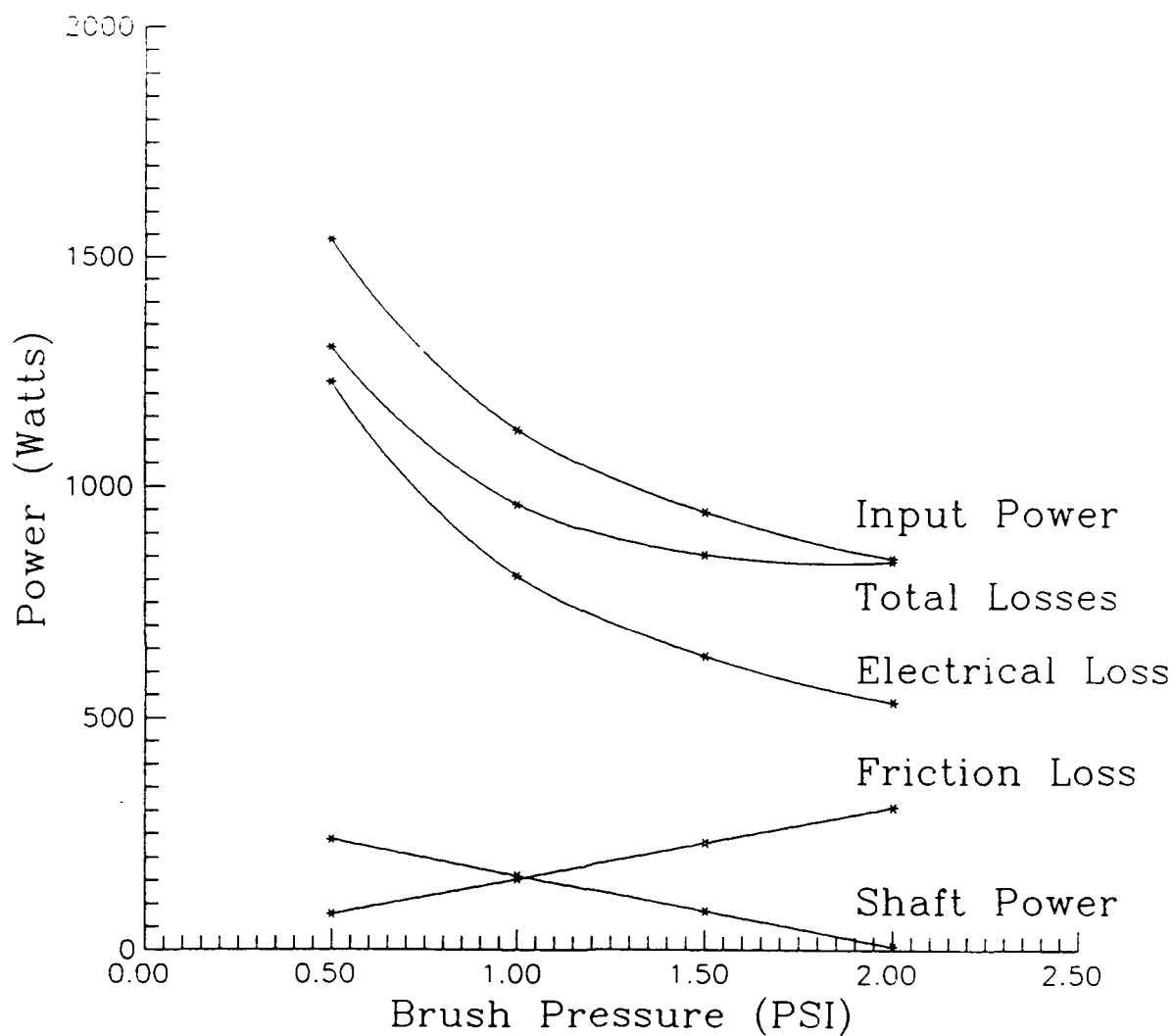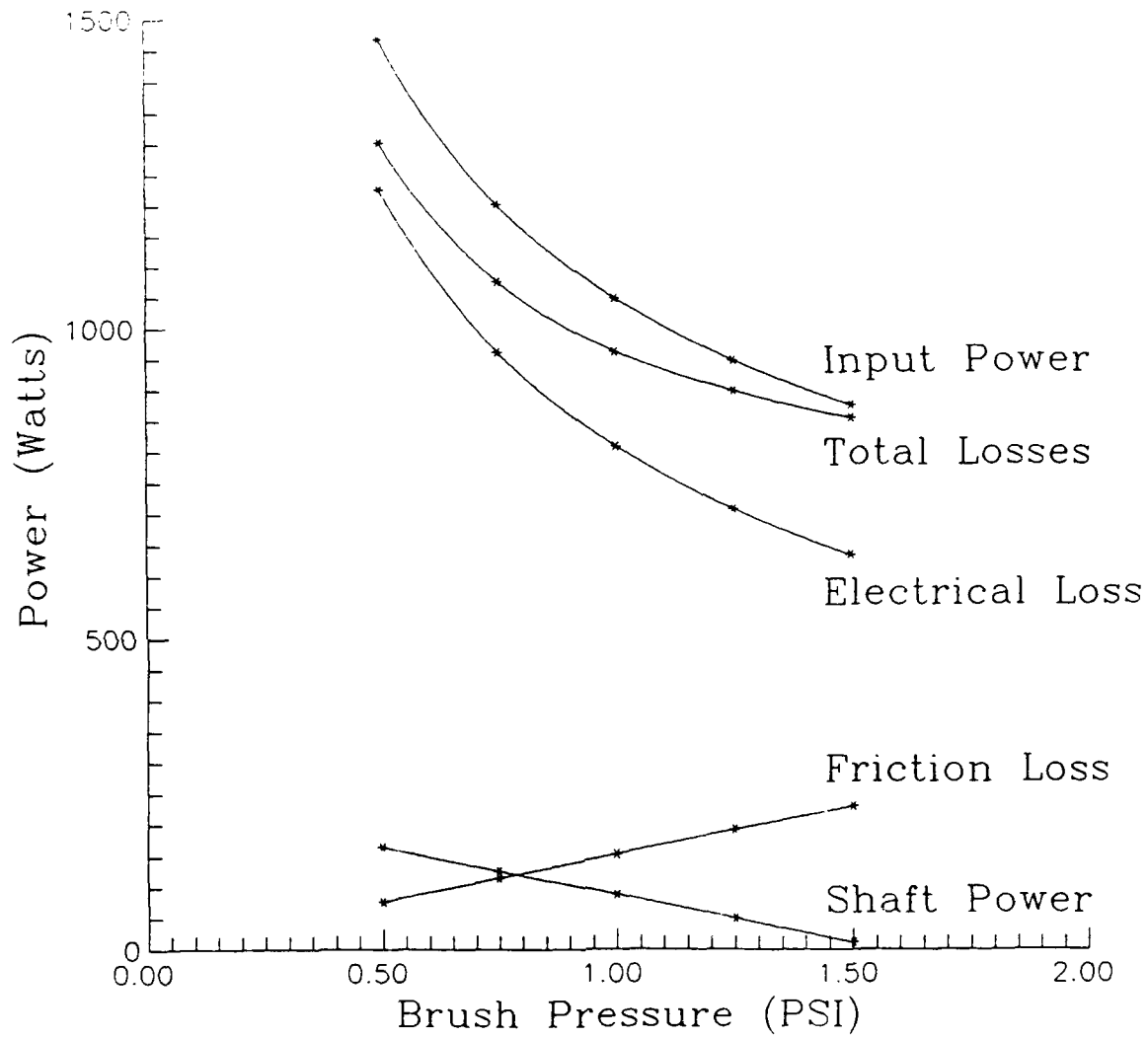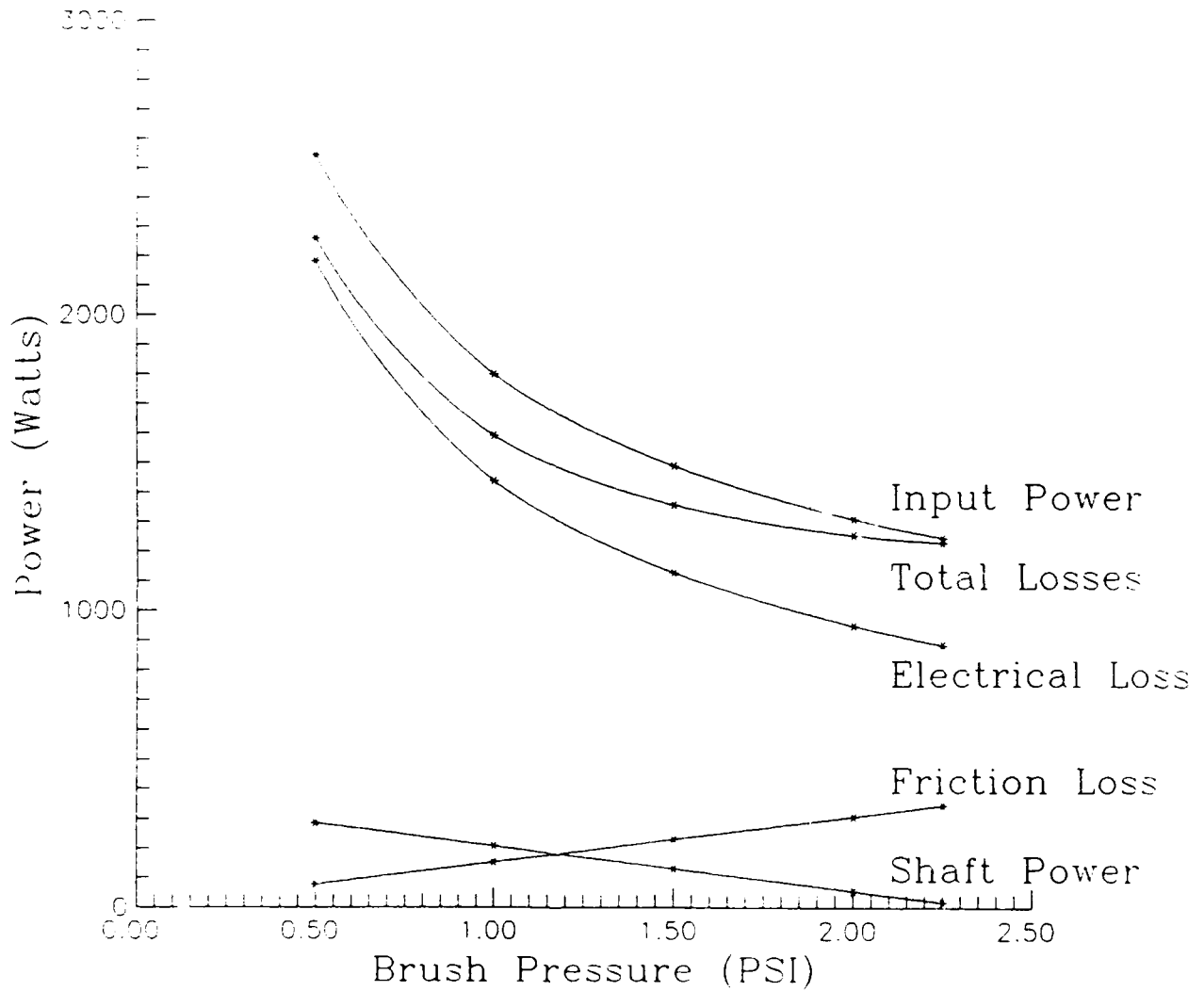
Figure 3.4 9 Motor Power and Losses Vs. Brush
Pressure for 20% Field Coil Ampere Turns.
Speed is 3000 RPM. Current is 1500 Amperes

springs to test the motor at various brush pressures. If the brushes are too lightly loaded, we may have arcing problems.

As wire properties improve, we can rewind the coils and operate closer to the full designed field performance.

3.5   Summary

Motor construction is progressing, with most parts either completed or on order. We completed the testing of two brush grades and various slip ring materials. The brush system will consist of brushes made of 85% copper and 15% graphite with a steel rotor that has 16 helical threads per inch in the slip ring area of brush contact. Finite element modeling of the flux and current distribution has improved our ability to calculate torque and predict the motor performance. The results are reported. Motor performance has been calculated based on reduced magnetic field levels due to low J_c values in a magnetic field. The results are reported and shown graphically.

SECTION 4

GENERAL DISCUSSION AND SUMMARY

The prototype motor is nearly finished, and soon will be ready to accept the nominal 575 Ampere-turn HTSC coils. Prototype HTSC wire has been produced in quantities sufficient to prove the feasibility of the green fiber process. The program is now graduating from a period in which we needed to merely make some wire to demonstrate a concept, and moving into a period when we must make operating hardware to demonstrate usefulness.

The major task in the coming months is to scale up the wire process to produce wire for the coils. This will be a big job, both in terms of the quantity of the wire and the electrical performance of the wire. The nominal coil design is based on about 4600 turns of monofilament HTSC wire rated at 0.125 amps (the current rating is small for fine diameter filaments). Each coil requires about 3000 meters of monofilament wire, executed as six separate windings of 500 meter lengths. With the furnace extension our capacity will be 20-50 meters per day per line, and with the anticipated four lines we can make 80-200 meters of spliced wire per day. Each 500 meter winding will involve 3-7 days of furnace time, or 2-3 months to pr duce the two coils. While this is a large scale-up from our present capability, it is clearly achievable. We also may increase the capacity by running more parallel lines of filaments through the furnace, or by learning how to reduce the time required for binder burnout and sintering.

Meeting the design performance of the coil will be a challenge. The output of the motor depends directly on the strength of the field coils, which are entirely determined by the J_c vs. B characteristics of __long__ lengths of the wire. The calculated motor performance is realistic, since it is based on actual __short__ wire data, but it is likely that the critical current density of a 3000 meter wire will be different from a 20 mm sample. To make field coils in the mid-1990 time period we have a very important short term focus to get the best possible performance from the existing sintered Y-123 wire. The coil performance will be significantly improved if we can achieve even small increases in J_c at 100 G.

The directionally solidified Y-123 wire and the BiSCCO wire promise improved $J_c(B)$ behavior in the near future, but certainly will not be available in kilometer lengths for winding field coils in 1990. Nevertheless it is an extremely important challenge. The 575 amp-turn coil is important only for our 1990 demonstration motor. Strong link wire is needed for real applications.

SUMMARY

Wire development focussed on improving and scale-up of the fiber spinning and green cladding process steps. Co-firing development emphasized determining optimal burnout and firing conditions on one meter-long wire samples, while the continuous reel-to-reel sintering was down during a major expansion of the furnace. The scope of materials was widened beyond phase pure Y-123, as we explored Y-123 alloyed with CuO, Y-211, and $BaCuO_2$, the newer Y-124 material, and BiSCCO powders.

Much progress was made in the green fiber areas. A 1.5 kilometer spool of continuous 125-micron fiber was produced, representing nearly a five-fold increase in fiber length. Higher solids loaded fibers containing 60 volume percent Y-123 was further developed using the polyethylene carrier polymer. Potentially better carrier polymers were explored. Green fiber braiding, necessary for multifilamentary wire, progressed from eight-filament round braids of 175-micron fiber to sixteen filament flat braids of 125-micron fiber.

The green cladding operation was significantly improved, as silver alloy coatings were produced with much better adhesion, thickness control, and uniformity. The apparatus was upgraded to nearly eliminate certain cladding defects. The scale of the green cladding operation was increased more than ten-fold with the production of a 0.53 kilometer long continuous green clad fiber. Several problems involving reactions with the silver alloys were uncovered and overcome.

Using meter-long samples, the burnout and sintering conditions for bare fiber and clad wire were systematically explored. This led to improvements in transport critical current density to values as high as 2800 A/cm^2. Design was completed and construction begun on a 3.3 meter long extension to the continuous sintering furnace. This will increase the size of the furnace from the present 3-zone/0.6 meter long hot section up to 8-zone/3.4 meter long hot zone. This will significantly increase residence time and allow binder burnout and sintering to be done in a single pass. This will permit the production rate of continuously sintered wire to be increased by a factor of 8-16.

A more reliable specimen mounting method improved the transport critical current measurement technique, allowing us to measure more specimens. This provided faster feedback data on the effect of processing conditions on J_c, and

encouraged measurements of many replicate specimens. The multiple replicate data is used to determine the statistical variation of J_c. Self field data is now routinely compared with data in applied magnetic fields. Magnetic susceptibility measurements are being done as a routine procedure.

Efforts increased on development of melt processing to produce high critical current density wire. A directional solidification program is beginning involving laser melting at Arthur D. Little with crystal growth and characterization support from Oak Ridge National Laboratory. Rapid thermal processing developments continue in collaboration with Sandia National Laboratory.

The construction of the first generation drum homopolar motor is in progress, with most parts completed or on order. A design for a nominal 575 ampere-turn HTSC coil has been specified. The brush system for current collection has been designed and the performance of the brush and slip ring system has been tested in liquid nitrogen. The brush system will consist of 85% copper-15% graphite brushes on a helical threaded steel rotor. Torque and motor performance has been calculated from finite element modeling of flux and current distribution.

Motor performance is predicted using reduced magnetic field levels based on the actual $J_c(B)$ behavior of wire samples. Motor power and losses have been calculated. The efficiency of the first machine will be very low, due to the quite small magnetic fields which will be produced by the HTSC field coils. Brush pressure is a major parameter affecting the losses, since the electrical losses from contact voltage drop decrease with pressure, while friction losses increase with pressure. Optimal brush pressure has been predicted for several values of current and field coil ampere turns.

REFERENCES

1. M. R. Chadrachood, I. S. Mulla, and A.P. B Shinha, Applied Physics Letters 55 (14) 2 October 1989 pp 1472-1473

2. Liu Hongbao, et al., Solid State Communications, 69 **(8)** pp.867-868 (1989)

3. Sungho Jin et al., presentation at the Materials Research Society meeting December 1, 1989, Boston, MA

4. O. Kubaschewski and C. B. Alcock, <u>Metallurgical Thermochemistry</u>, Fifth Edition, Pergamon Press 1979, p.386

5. M. Okada, et al., "Improvement of Grain Boundary Weak-links in Tape Shaped Wire Prepared by the Unidirectional Solidification Technique", presented at the Materials Research Society Meeting, Boston, MA, December 1, 1989

6. E. Yanagisawa et al., "Synthesis of Unidirectionally solidified Y-Ba-Cu-C Bulk Superconductors with High Critical Current Densities", Presented at the Materials Research Society Meeting, Boston, MA, November 28, 1989

7. D.S. Ginley, J.F. Kwak, M. Mitchell, J.W. Halloran, and M. Neal, "Rapid Thermal Processing of Y-123 Spun Wires", Applied Physics Letters, in press (1990)

ATTACHMENT I

REPORT SUMMARY

COMPOSITE CERAMIC SUPERCONDUCTING WIRES FOR ELECTRIC MOTOR APPLICATIONS

Sixth Quarterly Report on
Contract Number N00014-88-C-0512

January 31, 1990

John W. Halloran, Ceramics Process Systems Corporation, Milford, MA 01757

This report describes progress on developing Y-123 wire for an HTSC motor. The wire development activity includes synthesis of Y-123 powder, spinning polymer-containing "green fiber", heat treating the fiber to produce metallized superconducting filaments, and characterizing the electrical properties of the filaments. Green fiber is produced in lengths up to 1.5 kilometers, and metallized as "green clad" fiber at lengths of 0.5 kilometers. The green clad fiber is converted to silver-clad superconducting wire by a sintering operation.

The sintered wire has a $J_c(77°)$ up to 2800 A/cm^2 in self field, dropping to low values in magnetic fields. Directional solidification efforts are underway to improve the critical current density.

The construction of the first prototype HTSC homopolar motor is in progress. The design specifies a 575 ampere-turn HTSC coil. The current collection system has been tested in liquid nitrogen. Motor performance has been predicted based on actual $J_c(B)$ behavior of wire samples. Motor power and losses have been calculated. The efficiency of this initial machine is limited by the magnetic fields obtainable from present HTSC wire coils.

This report describes progress on developing Y-123 wire for
an HTSC motor. The wire development activity includes synthesis of
Y-123 powder, spinning polymer-containing "green fiber", heat
treating the fiber to produce metallized superconducting filaments,
and characterizing the electrical properties of the filaments.
Green fiber is produced in lengths up to 1.5 kilometers, and
metallized as "green clad" fiber at lengths of 0.5 kilometers. The
green clad fiber is converted to silver-clad superconducting wire
by a sintering operation.

The sintered wire has a $J_c(77°)$ up to 2800 A/cm^2 in self field,
dropping to low values in magnetic fields. Directional
solidification efforts are underway to improve the critical current
density.

The construction of the first prototype HTSC homopolar motor
is in progress. The design specifies a 575 ampere-turn HTSC coil.
The current collection system has been tested in liquid nitrogen.
Motor performance has been predicted based on actual $J_c(B)$
behavior of wire samples. Motor power and losses have been
calculated. The efficiency of this initial machine is limited by
the magnetic fields obtainable from present HTSC wire coils.

ARPA ORDER NUMBER: 9525   PROGRAM CODE NUMBER: 7737

CONTRACTOR: Ceramic Process Systems Corporation
                155 Fortune Boulevard
                Milford, MA 01757

CONTRACT NUMBER:N00014-88-C-0512   CONTRACT AMOUNT: $ 5,509,387

EFFECTIVE DATE OF CONTRACT: 30 JUNE 1988

EXPIRATION DATE OF CONTRACT: 31 MARCH 1991

PRINCIPAL INVESTIGATOR: John W. Halloran

TELEPHONE NUMBER: (508) 634-3422

SHORT TITLE OF WORK: High Temperature Superconducting Wire and Motor

REPORTING PERIOD: 1 October 1989 through   31 December 1989

DESCRIPTION OF PROGRESS

     This report describes progress on producing Y-123 wire for an HTSC motor. Wire development focussed process improvement and scale-up. During the down time associated with a major expansion of the continuous sintering furnace, efforts were aimed at optimizing the sintering process of one meter-long wires.   The scope of materials was widened beyond phase pure Y-123, as we explored Y-123 alloyed with other phases, the newer Y-124 material, and BiSCCO powders.
     Good progress was made in the green fiber areas.   A 1.5 kilometer spool of continuous 125-micron fiber was produced, representing nearly a five-fold increase in fiber length.   Green fiber braiding, necessary for multifilamentary wire, progressed from eight-filament round braids of 175-micron fiber to sixteen filament flat braids of 125-micron fiber.
     The green cladding operation was significantly improved, as silver alloy coatings were produced with much better adhesion, thickness control, and quality. The scale of the green cladding operation was increased more than ten-fold with the production of a 0.53 kilometer long continuous green clad fiber.   Using meter-long samples, the burnout and sintering conditions for bare fiber and clad wire were systematically explored.   This led to improvements in transport critical current density to values as high as 2800 A/cm . Design was completed and construction begun on a 3.3 meter long extension to the continuous sintering furnace to increase the length of the heated sections by more than a factor of five, adding five more controlled temperature zones. With the increased residence time binder burnout and sintering to be done

in a single pass, which can increase the production rate of continuously sintered wire by a factor of 8-16.

A more reliable specimen mounting method provided faster feedback data on the effect of processing conditions on J_c, and encouraged measurements of many replicate specimens. The multiple replicate data is used to determine the statistical variation of J_c. Magnetic susceptibility measurements are being done as a routine procedure.

Efforts increased on development of melt processing to produce high critical current density wire. A directional solidification program is beginning involving laser melting at Arthur D. Little with crystal growth and characterization support from Oak Ridge National Laboratory. Rapid thermal processing developments continue in collaboration with Sandia National Laboratory.

The construction of the first generation drum homopolar motor is in progress. A design for a nominal 575 ampere-turn HTSC coil has been specified. The performance of the brush and slip ring current collection system has been tested in liquid nitrogen. Torque and motor performance has been calculated from finite element modeling of flux and current distribution.

Motor performance is predicted using reduced magnetic field levels based on the actual $J_c(B)$ behavior of wire samples. Motor power and losses have been calculated. The efficiency of the first machine is limited by the small magnetic fields obtainable fr n present HTSC field coils.

SUMMARY OF SUBSTANTIVE INFORMATION DERIVED FROM SPECIAL EVENTS
Project members attended the several conferences on high temperature superconductivity to keep abreast of current developments.

CHANGE IN KEY PERSONNEL: No change

PROBLEMS ENCOUNTERED AND/OR ANTICIPATED: None

ACTION REQUIRED BY THE GOVERNMENT: None

FISCAL STATUS (December 31, 1989)

1) CUMULATIVE AMOUNT CURRENTLY RECEIVED
ON CONTRACT . . . . $ 2,334,172

2) CUMULATIVE EXPENDITURES AND
COMMITTMENTS TO DATE . . . . $ 2,545,456

3) ADDITIONAL FUNDS REQUIRED TO COMPLETE WORK

THROUGH FY 1990 . . . . $ 1,682,540